Analysis of the air cargo transport network using a complex network theory perspective

Bombelli, Alessandro; Santos, Bruno F.; Tavasszy, Lorant

DOI
10.1016/j.tre.2020.101959

Publication date
2020

Document Version
Final published version

Published in
Transportation Research. Part E: Logistics and Transportation Review

Transportation Research Part E 138 (2020) 101959

Contents lists available at ScienceDirect

Transportation Research Part E

journal homepage: www.elsevier.com/locate/tre

Analysis of the air cargo transport network using a complex network theory perspective

Alessandro Bombelli[a,b,*], Bruno F. Santos[a], Lóránt Tavasszy[c,b]

[a] Air Transport and Operations, Faculty of Aerospace Engineering, Delft University of Technology, Building 62 Kluyverweg 1, 2629 HS Delft, Netherlands

[b] Transport & Planning, Faculty of Civil Engineering and Geosciences, Building 23 Stevinweg 1, 2628 CN Delft, Netherlands

[c] Engineering Systems and Services, Faculty of Technology, Policy and Management, Building 31 Jaffalaan 5, 2628 BX Delft, Netherlands

ARTICLE INFO

Keywords:
Air cargo transport network
Complex network theory
Integrators
Network topology
Network robustness
Hub-and-spoke
Betweenness centrality

ABSTRACT

In this paper, we present a complex network analysis of the air transport network using the air cargo, instead of the passenger, perspective. To the best of our knowledge, this is the first work where a global cargo network comprising passenger airlines, full-cargo airlines, and integrators' capacity was studied. We used estimated yearly cargo capacity between airport pairs as input to the model. After assessing network characteristics of the sub-networks representing different carrier types, the full network was obtained as a super-imposition of the individual sub-networks. The resulting network has both small-world and scale-free characteristics. Its topological properties resulted in a higher flow imbalance and concentration with respect to its passenger counterpart, with a smaller characteristic path length and diameter. This result is consistent with the larger catchment area of cargo airports, which heavily rely on road feeder services for the ground leg. Finally, we showed how different attack strategies result in hubs of hub-and-spoke systems or airports behaving as bridges between communities being attacked first. We believe this work to be of relevance both for academics and for practitioners in an era where, due to the soaring of e-commerce and next day delivery, new players are entering the air cargo business and competition is constantly increasing.

1. Introduction

Although only 1% of the total volume of the world trade is transported via air, the orientation towards high value products results in a share of almost 35% of international trade value (IATA, 2020a). This trade value exceeded 6.2 trillion dollars in 2018, representing 7.4% of the world GDP. The air cargo supply chain is essential to many facets of everyday life. As example, the transport of perishable goods from one side of the planet to the other can be effectively carried out only via air cargo transport. Other sectors that heavily rely on air cargo transportation are the pharmaceutical industry, the high-tech industry and the e-commerce (IATA, 2020b).

Notwithstanding this relevance, the air cargo business is generally regarded as of secondary importance with respect to its passenger counterpart. This is also reflected in the academic literature, with an imbalance between works addressing passenger and cargo air networks. The complexity of the air cargo supply chain, that involves more stakeholders with conflicting goals, and the simultaneous presence of passenger airlines, full-cargo airlines, and integrators, partially justifies this imbalance.

* Corresponding author at: Air Transport and Operations, Faculty of Aerospace Engineering, Delft University of Technology, Building 62 Kluyverweg 1, 2629 HS Delft, Netherlands.

E-mail addresses: a.bombelli@tudelft.nl (A. Bombelli), b.f.santos@tudelft.nl (B.F. Santos), l.a.tavasszy@tudelft.nl (L. Tavasszy).

https://doi.org/10.1016/j.tre.2020.101959
Received 29 May 2019; Received in revised form 6 April 2020; Accepted 18 April 2020
Available online 20 May 2020
1366-5545/

In this paper we provide, to the best of our knowledge, the first complex network analysis of a worldwide air cargo network, named Air Cargo Transport Network (ACTN). A complex network is a network whose topological characteristics are non-trivial, and do not generally occur in basic networks such as random graphs. Complex network theory has been widely applied in the last couple of decades to a variety of real-world systems that can be modeled as complex networks (Barabási and Albert, 1999; Barabási, 2009; Strogatz, 2001). In particular, the development of the Internet (Cohen et al., 2000) and, more recently, of social media has provided a strong boost to the research field. Transportation-inspired networks, as the ACTN is, are another natural application field for complex network theory.

We built the ACTN embracing the air cargo perspective, using estimated yearly cargo capacities between Origin-Destination (OD) airport pairs as input to our complex network theory analyses. We also highlight two factors that were identified as distinctive of the air cargo transport network when compared with its passenger counterpart.

1. Cargo operations are more concentrated than passenger operations, relying more on hub-and-spoke structures and involving a smaller number of airports. While passengers generally choose airports within a 1 h radius from their origin or destination, the catchment area for air cargo transport extends to a 12 h radius (Boonekamp and Burghouwt, 2017) because it relies on Road Feeder Services (RFS) for the ground leg. This means that a smaller number of airports can be used to cover the same delivery area. In addition, cargo handling and consolidation needs an additional logistics layer, which comprises dedicated warehouses and ground handlers, special temperature-controlled rooms for perishable products, etc, that not all airports have.
2. The number of connections with other airports is not the best proxy to assess the relevance of an airport in the air cargo transport network. Notwithstanding a correlation between the two factors, the cargo business is characterized by a great imbalance in the amount of transportable goods (Boonekamp and Burghouwt, 2017). This imbalance in demand is particularly relevant for passenger airlines, that use a combination of full freighters and belly capacity (Bowen, 2012). Rather than the number of connections, what should be assessed is the overall cargo capacity that those connections can provide.

Our contribution is twofold. First, we characterize for the first time a global air cargo transport network, where all the main contributors (i.e., passenger airlines, full-cargo airlines, integrators) are considered. Second, we use a complex network framework to characterize topological and robustness features of the ACTN and identify similarities and differences with respect to the passenger counterpart.

The rest of the paper is organized as follows. Section 2 provides an overview of the literature pertaining complex network theory applied to transportation. Section 3 presents the complex network indices that are used in the paper. Section 4 describes that datasets used to build the ACTN and provides a preliminary spatial description of the network. Section 5 focuses on a thorough description of the topological properties of the network. In Section 6 the role of different airport types is assessed and compared using complex network theory indices. Finally, Section 7 provides conclusions and recommendations for future work.

2. Literature review

Given the nature of this paper, we will focus on complex network theory applications that specifically addressed transportation problems. For a more general framing of complex network theory, or for applications spanning other research areas, we refer readers to the references we provided in Section 1. For transport applications, we will cover urban, railway, and maritime systems in this sequence, and conclude with a more in-depth analysis of works addressing air transport networks.

Complex network theory has been applied to urban street patterns to unravel analogies between centrality measures and topological properties of the urban layout. In Crucitti et al. (2006), urban street patterns of different cities around the world were studied and compared using four centrality measure indices. In particular, it was shown that self-organized cities exhibit properties similar to those found in nonspatial networks, while planned cities do not. The work was complemented by Cardillo et al. (2006), where a comparative study of the urban layout of a set of twenty cities was carried out. For each planar graph, the structural properties were compared with those of the minimally connected and maximally connected planar graph generated from the original graph. Since cities were classified a priori into seven classes, results of the analysis were used to cluster cities and verify that the assignment closely matched the a priori categorization.

As it concerns rail transportation, Sen et al. (2003) focused on the Indian Railway Network (IRN) system and studied structural properties of the network from a complex network perspective. By using the mean distance in the network as a proxy to assess the goodness of the connectivity in the network, the authors showed that the mean distance of the IRN varies logarithmically with the number of nodes and a high clustering coefficient is achieved. As a consequence, the IRN displays small-world characteristics. A similar approach can be found in Latora and Marchiori (2002), where small-world characteristics of the Boston subway system were also highlighted.

Maritime networks have also been analyzed from a complex network perspective. In Kaluza et al. (2010), the Global Cargo Ship Network (GCSN) was studied as a network of ports that are connected by links if ship traffic passes between them, and scale-free properties were highlighted and compared with the ones of other transportation-inspired networks. In Ducruet et al. (2010), a network analysis of North Eastern Asian lines was performed, while (Ducruet and Notteboom, 2012) analyzed the relative position of ports in a global network through centrality indicators. (Calatayud et al., 2017) studied the vulnerability of international freight flows as a function of the multiple complex structure of the liner shipping network.

In the field of air transportation, complex network theory has been extensively applied using the perspective of passengers. The structure of the air transportation network has been studied both at the global and at the local scale. In Guimera and Amaral (2004)

and Guimera et al. (2005), the World-wide Airline Network (WAN) was thoroughly analyzed from a complex network perspective, and a network with similar topological properties was used in Verma et al. (2014). On the other hand, Cardillo et al. (2013), Malighetti et al. (2008), and Paleari et al. (2010) focused on the European air transport network, while (Wang et al., 2011; Du et al., 2016) presented two different models of the Chinese air transport network, the Air Transport Network of China (ATNC) and Chinese Airline Network (CAN), respectively. Previous works addressed the definition of the topological structures of the air transport networks (Guimera and Amaral, 2004; Du et al., 2016; Cardillo et al., 2013), the robustness of the network (Verma et al., 2014; Lordan et al., 2014), or the identification of multi-layered structures within the network (Verma et al., 2014; Du et al., 2016; Cardillo et al., 2013). In Malighetti et al. (2008), the connectivity of the European air transportation network was assessed using a time-dependent minimum path approach, while (Paleari et al., 2010) is an extension of the previous work where the connectivity of the air networks of China, Europe, and United States was compared. The large number of works addressing air networks from the passenger perspective can be appreciated in Burghouwt and Redondi (2013), where eight different models are compared. We refer readers to this work for further reading and references. To the best of our knowledge, the air cargo perspective has never been explicitly adopted when analyzing a global air transport network with complex network theory. The only works we are aware of are (Bowen, 2012), where the network topology of integrators FedEx and UPS was analyzed in terms of number of nodes (airports) and edges (undirected connections between airports), and (Malighetti et al., 2019), where the network topology of integrators FedEx, UPS, and DHL (limited to their Asian network) was assessed.

3. Overview of complex network theory indices

We model the ACTN as a directed graph $\mathcal{G} = (\mathcal{N}, \mathcal{E})$, where $\mathcal{N}$ is the set of nodes (airports), and $\mathcal{E}$ is the set of directed edges (connections between $\mathcal{OD}$ airport pairs). As the following sections will reveal, triangular routes and capacity imbalances in the air cargo business make this approach more suitable than the undirected one. In a graph, edges can be *unweighted* (i.e., characterized by the same weight), and in this case they are generally assigned a unitary value, or *weighted*, where the weight depends on the properties of $\mathcal{G}$. Note that, in network theory, there is a clear distinction between an edge *weight* and *cost*. The former, also known as strength (Brandes, 2001; Newman and Girvan, 2004), has a "positive" connotation, while the latter has a "negative" connotation and is the characteristic to be used when computing shortest paths in $\mathcal{G}$. As example, traffic flows or capacities generally define weights, while distance (Euclidean or not) is the most natural example of cost.

An unweighted directed graph is mapped with an adjacency matrix that is a binary matrix $\mathcal{A}_{|\mathcal{N}|\times|\mathcal{N}|}$, where $a_{ij} = 1$ if a directed edge connects nodes i and j. All the nodes j that are reachable from a node i with a single step, i.e., $a_{ij} = 1$, are its neighbors. If the graph is weighted, $\mathcal{A}$ is replaced with the weight matrix $\mathcal{W}$, where w_{ij} represents the weight of the directed edge pointing from i to j. Throughout the paper, we will be using indices that are node-, edge-, or network-specific, and whose description is provided hereafter.

The *in-degree* of node i is $k_{in}(i) = \sum_{j=1}^{|\mathcal{N}|} a_{ji}$ and identifies the number of nodes with a connection to node i. The *out-degree* of node i is $k_{out}(i) = \sum_{j=1}^{|\mathcal{N}|} a_{ij}$ and identifies the number of nodes reachable from node i (i.e., it is the cardinality of the set of neighbors of node i). We define the degree of node i as $k(i) = k_{in}(i) + k_{out}(i)$. If $n(\bar{k})$ is the number of nodes in the network with a degree equal to $\bar{k}$, the cumulative degree distribution

$$P(>\bar{k}) = \frac{\sum_{t=\bar{k}}^{\infty} n(t)}{|\mathcal{N}|} \tag{1}$$

expresses the ratio of nodes in the network with a degree greater or equal to $\bar{k}$. The *strength* $s(i)$ of node i is defined as $s(i) = \sum_{k=1,k\neq i}^{|\mathcal{N}|} a_{ki}w_{ki} + \sum_{k=1,k\neq i}^{|\mathcal{N}|} a_{ik}w_{ik}$, i.e., it is the summation of the weights of all edges entering/exiting node i. The normalized *local clustering coefficient* $C(i)$ (Fagiolo, 2007) of node i in a directed graph is defined as

$$C(i) = \frac{(\mathcal{A} + \mathcal{A}^T)^3_{ii}}{2[k(i)(k(i)-1) - 2k(i)^{\leftrightarrow}]} \tag{2}$$

where $k(i)^{\leftrightarrow} = \mathcal{A}^2_{ii}$ is the number of neighbors of node i for which i is a neighbor. The closer $C(i)$ is to the unitary value, the more connected the neighbors of node i are. In a fully-connected graph, $C(i) = 1\ \forall\ i \in \mathcal{N}$. The normalized *betweenness centrality* (Freeman, 1977) $g(i)$ of node i is defined as

$$g(i) = \frac{1}{(|\mathcal{N}|-1)(|\mathcal{N}|-2)} \sum_{i\neq j\neq k} \frac{\sigma_{jk}(i)}{\sigma_{jk}} \tag{3}$$

where σ_{jk} is the number of shortest paths between nodes j and k, and $\sigma_{jk}(i)$ is the number of those paths passing through node i. The normalization term in Eq. (3) accounts for the fact that paths starting or ending in i are not considered. This index correlates the relevance of a node with the frequency the node appears in shortest paths that neither start nor end in i. Another node-specific index we present is *closeness centrality* $c(i)$ of node i, defined as

$$c(i) = \frac{2(|\mathcal{N}|-1)}{\sum_{\substack{j=1 \\ j\neq i}}^{|\mathcal{N}|} (d_{ij} + d_{ji})} \tag{4}$$

where d_{ij} is the shortest path, measured in number of steps, from node i to node j. This measure represents the inverse of the average unweighted shortest path from/to the current node to/from any other node, and defines the accessibility of a node in the network. If a node is directly connected to every other node in the network, and vice versa, closeness centrality has a unitary value. We conclude the overview of node-specific indices introducing the *modal contribution* (Petreska et al., 2010) $w(i)$ of node i, defined as

$$w(i) = \sum_{i=1}^{|\mathcal{N}|} |\Gamma_{ij}| \tag{5}$$

where $\Gamma = \mathcal{L}'\Phi$ is the modal connectivity matrix, with $\mathcal{L}$ the Laplacian matrix of $\mathcal{G}$ and Φ a matrix whose columns are the eigenvectors of $\mathcal{L}$. When computing $\mathcal{L}$, node strength $s(i)$ is used as weight. The modal contribution $w(i)$ is inspired by structural modal analysis and can be interpreted as a busyness measure of each node. In fact, considering the analogy between a graph and a system of mass-spring oscillators, we can express the system of net forces acting on the nodes as $\mathbf{F} = -\mathcal{L}\mathbf{X}$, that is the graph-inspired equivalent of the classic oscillator equation $\mathbf{F} = \omega^2\mathbf{MX}$ (Petreska et al., 2010). Modal contribution quantifies how a perturbation on a node (e.g., its removal) moves along the network similarly to a wave signal, and what its effects on the system are.

The only edge-specific index we will use in the paper is the normalized *edge betweenness centrality* (Girvan and Newman, 2002) $g_e(i)$ of edge i, defined as

$$g_e(i) = \frac{1}{|\mathcal{N}|(|\mathcal{N}|-1)} \sum_{i \neq j \neq k} \frac{\sigma_{jk}(i)}{\sigma_{jk}} \tag{6}$$

and that quantifies the relevance of edge i in $\mathcal{G}$ by assessing how often in appears in shortest paths. Since the focus is on edges and not on nodes, the normalization constant in Eq. (6) is different than the one in Eq. (3) because all combinations of nodes are considered. For both the normalized edge betweenness centrality and the normalized betweenness centrality, in the rest of the paper we will drop the term "normalized" when referring to the indices. In addition, the *density* of a graph is defined as the ratio between the number of edges and the maximum number of edges that can characterize such graph, i.e., $|\mathcal{E}|/(|\mathcal{N}||\mathcal{N}-1|)$. Another index that is specific for directed graphs is the *reciprocity*, defined as the ratio between node pairs with edges in both directions and node pairs connected by an edge in at least one direction.

When it comes to network-specific indices, some of them are averages of node-specific indices. To indicate the arithmetic mean, we will use the angle bracket notation $\langle\rangle$. As example, the *average degree* is $\langle k \rangle = \frac{1}{|\mathcal{N}|}\sum_{i=1}^{|\mathcal{N}|} k(i)$, while the average clustering coefficient, also known as *global clustering coefficient* (Opsahl and Panzarasa, 2009; Watts and Strogatz, 1998; Fagiolo, 2007) is $\langle C \rangle = \frac{1}{|\mathcal{N}|}\sum_{i=1}^{|\mathcal{N}|} C(i)$. We define the *characteristic path length* of a network as

$$\langle L \rangle = \frac{1}{|\mathcal{N}|(|\mathcal{N}|-1)} \sum_{i=1}^{|\mathcal{N}|} \sum_{\substack{j=1 \\ j \neq i}}^{|\mathcal{N}|} d_{ij} \tag{7}$$

Note that, given Eq. (7), we assume an unweighted graph. Another network-specific index is the diameter $D = \max(d_{ij})$, defined as the longest shortest path in the graph. The component of a graph is a subset of the graph where does exist a path between each pair of nodes belonging to the component. The *giant component* $\mathcal{G}_c$ is the component with the highest number of nodes. If a path exists between every node pair in the graph, the graph itself is the giant component.

We conclude this section by providing two network definitions based on the analysis of the aforementioned indices. (i) A *small-world* network is a network where $\langle L \rangle$ is small and $\langle C \rangle$ is large. As the name suggests, these two characteristics make it possible to reach, on average, every node from any other node with a low number of steps. (ii) A *scale-free* network is a network whose degree cumulative distribution follows a truncated power law. This implies that the degree distribution is right-skewed, with the majority of nodes characterized by a low degree, and a small number of nodes characterized by a significantly higher degree.

4. Datasets and geography of the air cargo transport network

The airport selection for the ACTN was based on a database provided by *Seabury Consulting* [1]. The database contained

- a list of airports characterized by a yearly international cargo throughput of 5,000 tonnes or higher.
- for the aforementioned list of airports, the yearly frequency per aircraft type for all different $O\mathcal{D}$ airport pairs

In Fig. 1, all airports considered in the ACTN are shown. For the full list of airports, with International Air Transport Association (IATA) and International Civil Aviation Organization (ICAO) codes as well as geographic coordinates, we refer readers to the ACTN dataset that is publicly available at the following link (https://doi.org/10.4121/uuid:5725add4-7fe8-41d1-a452-b1fc011e0bae). Note that, unless differently specified, in the rest of the paper we will describe airports using their IATA code.

The frequency data which we used refer to the year 2014. We could not work on more recent data provided by *Seabury Consulting*, because they were considered too recent and not accessible. This is consistent with the general scarcity of publicly available data related to air cargo for academic purposes, where confidentiality and competition are crucial factors. This applies both to passenger

[1] www.seaburygroup.com

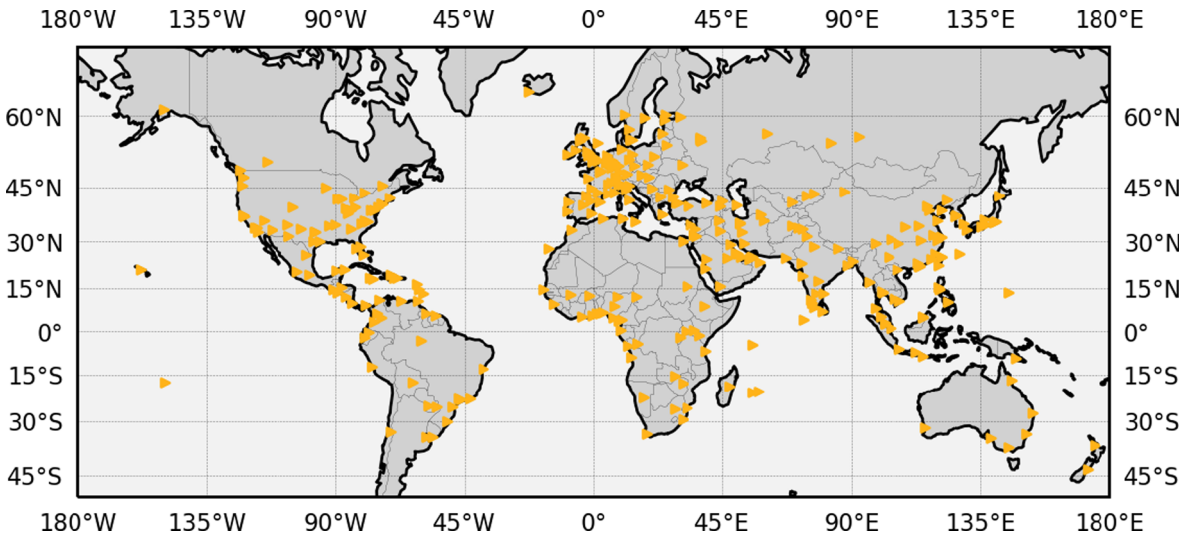

Fig. 1. Airports included in the ACTN.

airlines offering cargo services and, even more strongly, to integrators (Malighetti et al., 2019; Lakew, 2014). Along the same line, we retrieved integrator-specific data from 2019, as explained later in the section, because data from 2014 was not available. In both cases, we decided to rely on the most recent best dataset available. The implication of such an approach is that some integrator routes in the ACTN (especially from/to North Eastern Asia) might have been created after 2014. We believe this temporal inconsistency to have a small effect on the topology of the ACTN. In addition, results regarding the role of airports as described in Section 6 might be slightly affected, and could be re-computed provided more temporally consistent data availability.

The 5,000 tonnes threshold for cargo throughput was chosen by *Seabury Consulting* as a lower bound, to filter out airports whose contribution to the global cargo trade can be considered negligible. A yearly cargo flow of 5,000 tonnes is equivalent to a daily flow of 14 tonnes circa, which is the average belly cargo weight capacity of a single wide-body (WB) passenger aircraft. As it concerns the flight schedule database, narrow-body (NB) and WB full freighters, and WB passenger aircraft were considered. Passenger airlines were included, as well as all major cargo-only airlines such as Emirates SkyCargo, Singapore Airlines Cargo, Cargolux etc. Among minor cargo-only airlines, LATAM Cargo group did not report its frequencies. In addition, charters and other unscheduled operations, as well as integrators were not included in the dataset.

NB passenger aircraft were excluded from the *Seabury database* because deemed to provide a small contribution to the overall air cargo network. NB aircraft are mainly used by (i) non-low cost carriers (LCC) airlines for short- and medium-haul national or continental connections, and (ii) LCC airlines. As example, in 2019 the 10 largest operators of Airbus NB jets were: - easyJet, - China Eastern Airlines, - China Southern Airlines, - American Airlines, - LATAM, - Delta Airlines, - AirAsia Malaysia, - IndiGo, - jetBlue Airways, - Lufthansa, where four of the ten carriers are LCCs. The reason why *Seabury Consulting* omitted NB passenger aircraft can be motivated as follows. For non-LCC airlines, given the reasonably short distances between airports, freight forwarders might prefer RFS to transport goods instead of relying on air transport. On the other hand, LCCs historically did not offer cargo services at all. While we wanted to use the *Seabury database* for its completeness in terms of WB passenger and cargo operations and NB cargo operations, we are aware that neglecting NB passenger operations is, to a certain extent, myopic. In fact, non-LCC airlines do offer cargo services, although their capacity per flight is limited. Additionally, in the last few years LCCs also started to offer cargo services. Southwest Airlines, as example, recently started to offer cargo services, although their yearly transport is still relatively small (AirCargoWorld, 2019) (less than 400,000 tonnes per year). This trend has been fostered by the bounded capacity, when compared with soaring demand, offered by full freighters due to their limited fleet size. On the other hand, belly space in passenger aircraft offers a more limited weight capacity per flight, but higher flexibility both in terms of frequencies and destinations. In potential follow-up works (e.g., in case we wanted to update the 2014 *Seabury database*), NB passenger aircraft will be included in the analysis. Table 1 shows an extract of the aforementioned *Seabury database*.

Table 1
Example of the flight schedule database.

O	$\mathcal{D}$	Aircraft type	Frequency
HKG	TPE	Airbus A330-300	4,756
…			
TPE	ANC	Boeing 747-400F	1,753
…			
MXP	TLV	Boeing B777-200ER	1

In order to account for integrators, which were not part of the original database, but do play a crucial role in the global air cargo transport network, we focused on the two major United States carriers (FedEx and UPS) and the major European carrier (DHL). According to a *Seabury* estimate, the combination of reported frequencies by passenger and full-cargo airlines contained in the *Seabury database*, combined with the integrators' frequencies, represents around 95% of the overall cargo flows. Given this combination, the remaining missing capacity is to be attributed to the aforementioned charters and other unscheduled operations, and minor cargo-only airlines not reporting their schedules. We also focused on one such airline, i.e., LATAM Cargo group, and included it in our global network. Given the less significant size of the LATAM Cargo group fleet and set of destinations, we will focus our attention and provide more information of the integrators' and major cargo-only sub-networks in the rest of the paper. We added more data on the LATAM Cargo group sub-network in our online dataset.

We included all major hubs serving each of the three integrators in our airport selection. While, in most cases, cargo hubs are also hubs from a passenger perspective, a few exceptions exist. As example, RFD (Chicago Rockford International Airport) mainly operates as a general aviation airport, and thus does not play a crucial role from a passenger perspective. On the other hand, it has been since 1994 one of the major hubs for UPS Airlines. Note that the *non-integrator sub-network* refers to a year (2014) that precedes the acquisition of TNT by FedEx. On the other hand, the data we used to build integrators' routes is from 2019 and, as such, does not contain TNT flights.

To collect integrators' data, we relied on the *Flightaware*[2] database, that stores historical departures and arrivals for each airport of the previous 14 days. For each airport part of the ACTN, we initially retrieved all the recorded departures. Each departure was characterized by a flight code, an aircraft code, a destination airport, a departure time, and an Estimated Time of Arrival (ETA). Table 2 shows an extract of such dataset for departures from ORD. Note that, at this stage of the data retrieval process, the dataset contains all recorded departures (also towards destinations not part of the ACTN).

For each origin airport, departures were split into singular $O\mathcal{D}$ airport pairs, compatibly with the airports belonging to the ACTN, and each subset of departures was filtered to identify integrator flights. For identification purposes, we focused on the *flight code* column. For FedEx and UPS, which (almost) entirely rely on their own fleet (Malighetti et al., 2019), we searched for flight codes containing, respectively, FDX (FedEx Express) and UPS (UPS Airlines). DHL, differently than the other two integrators, does not rely on a single airline. It employs a fleet of owned or co-owned airlines that operate under the DHL brand or livery, or relies on other airlines with lease contracts to fully accommodate its cargo demand. Note that FedEx and UPS rely on other airlines as well, but to a much lesser extent or for contingency reasons. FedEx employs a small fleet of ASL Airlines Ireland ATR 42-300F turboprobs for local transport within Canada. UPS, on the other hand, has an agreement with Western Global Airlines to sub-contract five McDonnell Douglas MD-11F aircraft for up to 30 days per year to accommodate temporary volume spikes (DC Velocity, 2020). For DHL, we searched for flights belonging to airlines operating directly or indirectly for the integrator. We filtered flight codes containing the following codes: AHK (Air Hong Kong), ABR (ASL Airlines Ireland), BCS (European Air Transport), BDA (Blue Dart Aviation), DAE (DHL Aero Expreso), DHK (DHL Air UK), DHX (DHL International Aviation ME), PAC (Polar Air Cargo), SOO (Southern Air). For flight codes of airlines that do not fly directly under the DHL umbrella, we only stored flights where the flight code-aircraft type combination suggested a DHL-operated flight. As example, ASL Airlines Ireland operates only four Airbus A300-600RF for DHL. For LATAM, we searched flight codes containing the following codes: LCO (LATAM Cargo Chile), LTG (LATAM Cargo Brasil), LAE (LATAM Cargo Colombia).

The data retrieval process was carried out thirteen consecutive times with a bi-weekly frequency, from July 30th 2019 to January 13th 2020. Hence, the overall dataset we assembled covers six months, from mid-June 2019 to mid-January 2020. Ideally, the data retrieval process should be repeated on a bi-weekly basis over a full year time-span to obtain a more accurate representation of yearly schedules. For time limitations, we did not follow such an approach in this work. Our overarching goal is to estimate yearly capacity for each integrator's network. This can be translated into (i) the identification of all connections among the considered set of airports, and (ii) the estimation of a yearly capacity for each connection. Having assembled six consecutive months of data, we believe condition (i) to be satisfied. Connections that are only flown during the spring, as example, might not be present. Since we are considering the peak season (November and December) in our dataset, where demand reaches a peak worldwide, we believe this effect to be of minor relevance. The inclusion of the peak season was also one of the drivers to address condition (ii), as described later in this section.

At this stage of the process, we defined five sub-networks, namely (i) *non-integrator sub-network*, (ii) *FedEx sub-network*, (iii) *UPS sub-network*, (iv) *DHL sub-network*, and (v) *LATAM sub-network*, each characterized by a subset of airports part of the ACTN, and a list of all the served $O\mathcal{D}$ airport pairs. For each sub-network and $O\mathcal{D}$ airport pair, we had the recorded aircraft types and frequency for a full year (sub-network (i)) or for six months (sub-networks (ii), (iii), (iv), and (v)). We estimated the yearly maximum cargo capacity per sub-network and $O\mathcal{D}$ airport pair by initially determining the list of different aircraft (passenger and full freighter) appearing in the sub-networks. For each aircraft type, we retrieved the maximum transportable cargo weight as specified by airlines' websites or other public sources. We decided to use weight, as opposed to volume, as the capacity indicator, because we perceived it to be a more direct proxy. We also acknowledge that, for some commodities and aircraft type, the volumetric limit might be reached before the weight limit. Electronics, as example, is a commodity type that generally shows this pattern. In Fig. 2, we report the maximum transportable weight for all the aircraft types considered. In Appendix A, we report each aircraft type, code, transportable tonnage, and the source we used to determine the tonnage.

For sub-network (i), yearly aircraft frequencies were multiplied by the associated maximum payload. For the other sub-networks,

[2] https://flightaware.com

Table 2
Example of data format for departure information retrieved from *Flightaware*.

Flight code	Aircraft type	Destination airport	Departure	ETA
AAL2302	B738	LaGuardia (KLGA)	Fri 13:45 CDT	Fri 16:16 EDT
AWI3810	CRJ2	Central Wisconsin (KCWA)	Fri 13:44 CDT	Fri 14:14 CDT
AAL1168	B738	San Diego Intl (KSAN)	Fri 13:43 CDT	Fri 15:21 PDT
ENY3929	E170	Dane Co Rgnl (KMSN)	Fri 13:42 CDT	Fri 14:01 CDT
SKW2995	CRJ7	Detroit Metro Wayne Co (KDTW)	Fri 13:41 CDT	Fri 15:22 EDT
AAL1408	B788	Dallas-Fort Worth Intl (KDFW)	Fri 13:40 CDT	Fri 16:04 CDT
ENY3412	E145	Indianapolis Intl (KIND)	Fri 13:40 CDT	Fri 15:13 EDT
SKW2962	CRJ7	Bishop Intl (KFNT)	Fri 13:39 CDT	Fri 15:15 EDT

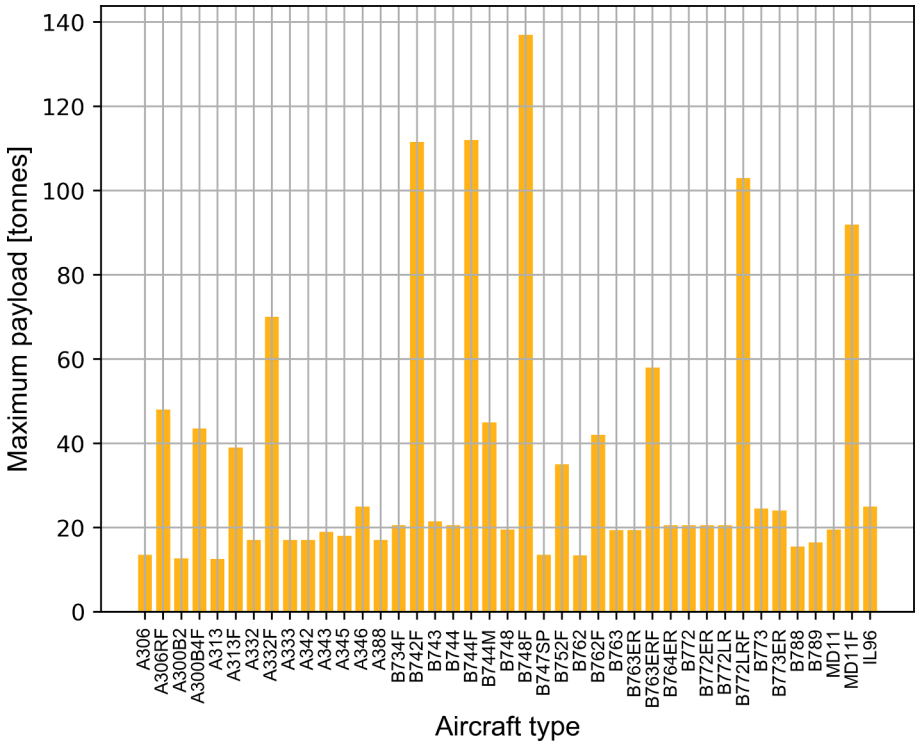

Fig. 2. Maximum payload for different passenger and full freighter aircraft.

we had to translate recorded capacities for six months into a full year, while acknowledging the potential non-uniformity of capacity because of seasonality effects. To gain some insights on such seasonality effects, we analyzed for each observation and each $\mathcal{OD}$ airport pair the estimated capacity. For each of the three integrators, in Fig. 3 we report the boxplots representing such estimated capacities for a subset of major routes, all having ANC as origin airport. Each data point in every boxplot refers to a bi-weekly observation, i.e., the associated value represents the cargo tonnage that was estimated to be flown from ANC to the intended destination in a 14-day time-span. Note that data points refer to consecutive and non-overlapping time-spans that cover the aforementioned 6-month period. In the rest of the paper, we will adopt the same terminology as in Malighetti et al. (2019), and define estimated capacity per $\mathcal{OD}$ airport pair as Available Freight Tonnes (AFT).

A good agreement in terms of AFT among different observations was found, also for connections not shown in Fig. 3. Notwithstanding the agreement, it can be noted the presence of some high-capacity outliers (black circles above the whiskers), that always corresponded to observations covering the first or second half of December, and some low-capacity outliers (black circles below the whiskers), that were more scattered during the summer period and September. The maximum variability among the routes shown was identified in the ANC-ORD flight leg for DHL. Interestingly, we noticed how some connections display a variation in the type and frequency of aircraft used according to the specific bi-weekly observation, while keeping the capacity level almost unchanged. Let us consider, as example, UPS flights from SDF to DEN referring to the two observations 13–27 August and 5–19 November 2019. In both cases, we identified Airbus A300-600F, Boeing 757-200SF, Boeing 767-300F, and McDonnell Douglas MD-11F as aircraft types, with a frequency of 23-3-16-2 (resp. 16-4-15-7). Given that the drop in Airbus A300-600F usage was compensated by a higher number of used McDonnell Douglas MD-11F, the estimated capacities for the two observations were, respectively, 2,300 and 2,400 tonnes.

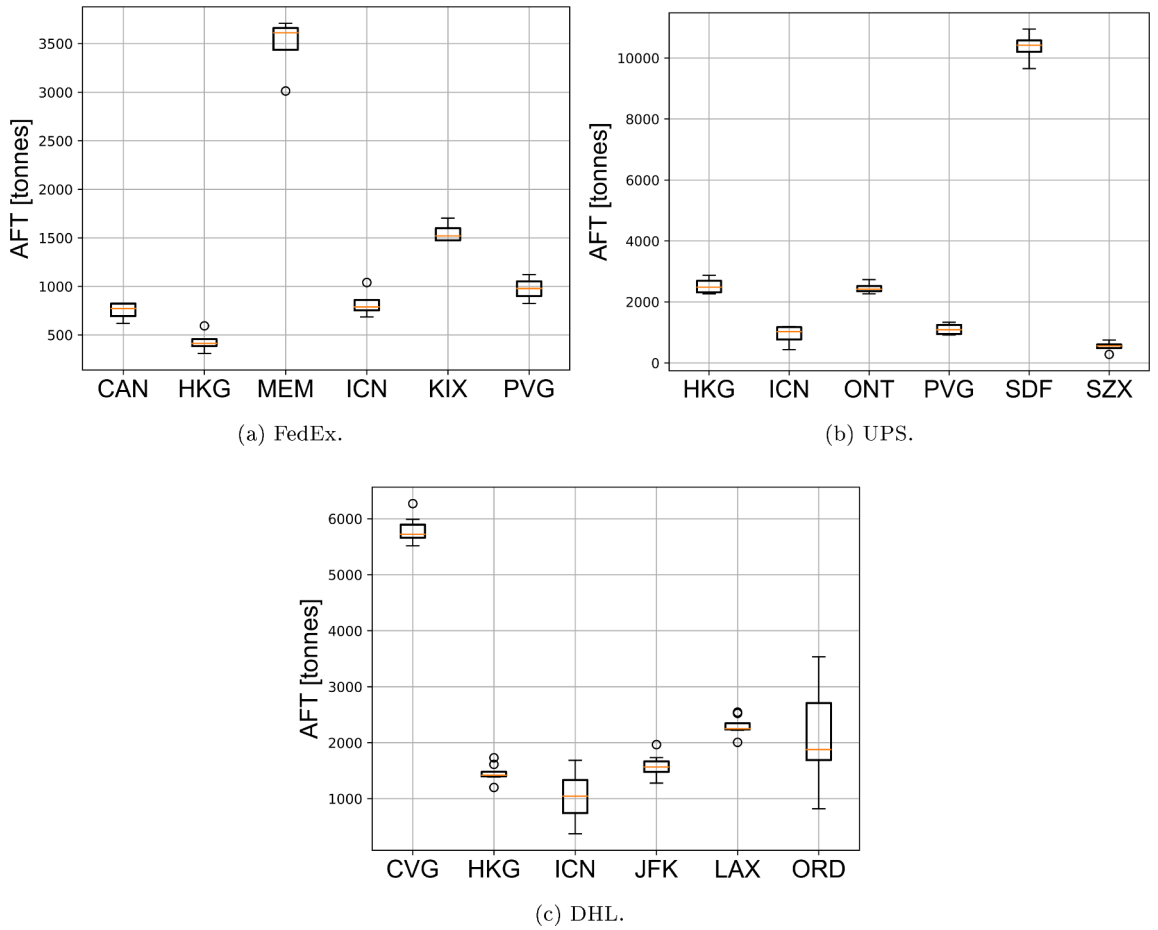

(a) FedEx.

(b) UPS.

(c) DHL.

Fig. 3. Boxplots representing AFT of different OD connections all originating in ANC.

To answer the original question regarding seasonality, we observed an average increase (considering all connections) between 5 and 8% in the available capacity for observations referring to late November and December: they correspond to the peak season that spans from Black Friday and Cyber Monday to Christmas (FreightWaves, 2019; ACI Blog, 2019). In light of seasonality effects that generally affects the fourth quarter of every year, which is fully included in our dataset, we estimated that our dataset represents 55% of the yearly integrator capacity. As such, to obtain an yearly AFT, each estimated capacity has been multiplied by a factor of 1/0.55. All the datasets with annual AFT are publicly available as part of our ACTN dataset (https://doi.org/10.4121/uuid:5725add4-7fe8-41d1-a452-b1fc011e0bae).

5. Topology of the air cargo transport network

5.1. Analysis of different sub-network types

The ACTN is represented as a directed graph $\mathcal{G} = (\mathcal{N}, \mathcal{E})$ that is the superimposition of the five sub-networks presented in Section 4. Before focusing on the ACTN, a complex network analysis of sub-networks (i), (ii), (iii), and (iv) is provided to gain some insights into the differences between a more passenger-oriented (*non-integrator sub-network*) and integrator-oriented networks, which might be harder to highlight in the full ACTN. Using the same methodology presented in Section 4, we also modeled a sub-network for Cargolux (*Cargolux sub-network*), a major European full-cargo airline with headquarters in LUX. Note that, while frequency data for Cargolux is already included in the *Seabury database*, the fact that data is not airline-specific would make it challenging to accurately extrapolate Cargolux-only information from it. We isolated all flights containing CLX (Cargolux Airlines International S.A.) or ICV (Cargolux Italia S.p.A.) in the flight code, and translated frequencies into an AFT. The reason why we decided to isolate such sub-network in this preliminary analysis, was to include an example of major full-cargo airline's network for comparison purposes with integrators' networks. In Fig. 4, the different sub-networks are shown. Note that we do not distinguish between unidirectional or bidirectional routes in the plots for sake of clarity. For the same reason, in the *non-integrator sub-network*, only the 1,000 connections with the highest AFT are reported.

In Table 3, the main characteristics of each sub-network are listed. As it concerns integrators, FedEx and UPS are more similar in

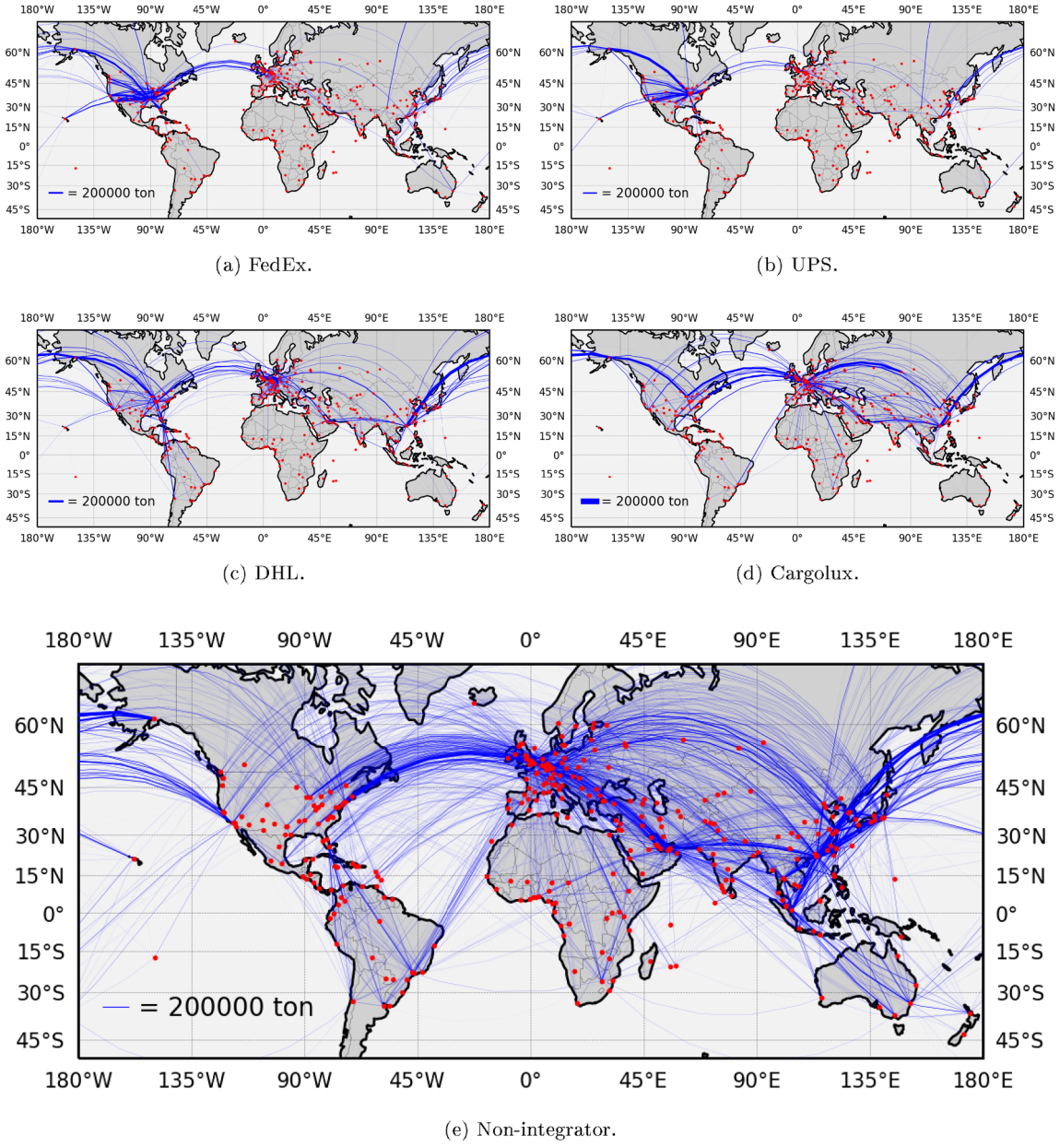

(a) FedEx.

(b) UPS.

(c) DHL.

(d) Cargolux.

(e) Non-integrator.

Fig. 4. Airports and routes for the *FedEx*, *UPS*, *DHL*, *Cargolux*, and *non-integrator sub-networks*.

Table 3
Comparison of *FedEx*, *UPS*, *DHL*, *Cargolux*, and *non-integrator sub-networks*.

	FedEx	*UPS*	*DHL*	*Cargolux*	*non-integrator*
Nodes	126	106	185	95	320
Edges	759	600	983	344	6,013
Density	0.048	0.053	0.029	0.039	0.059
Reciprocity	0.527	0.500	0.501	0.186	0.808
$\langle C \rangle$	0.552	0.482	0.419	0.407	0.501
$\lvert\mathcal{G}_c\rvert$	119	99	172	84	320
$\langle L \rangle$	2.4	2.5	2.6	2.1	2.4
D	5	8	8	6	5
Overall AFT	9,846,445	7,260,882	7,211,882	2,012,830	65,102,873
Overall AFTK	25,608,319,058	20,305,704,660	22,347,678,520	9,691,976,137	326,173,827,105

terms on nodes and edges than DHL, with the latter having a more developed network. We believe the difference resides in the set of smaller airlines that operate under the DHL livery, and enable the integrator to access second-tier cargo airports that are not part of the FedEx or UPS network. Along this line, the increment of airports reachable by DHL is not followed by an equal increment in the number of available connections, as the lower density of the DHL sub-network suggests. This outcome is consistent with what shown in Malighetti et al. (2019) for the Asian DHL network, described as more concentrated and less flexible and robust with respect to the FedEx and UPS counterparts. For the other parameters, i.e., reciprocity, global clustering coefficient, average shortest path, and diameter (the last two parameters computed considering the giant component of each sub-network), the three sub-networks show a high degree of consistency. In terms of AFT, FedEx is characterized a maximum capacity that is 25–35% higher than the one of its competitors. The same outcome is obtained if we consider the Available Freight Tonnes Kilometer (AFTK), which are computed multiplying each AFT by the great circle distance between the origin and destination airport. In particular, for FedEx we obtained 25.6 trillion tonnes·km, and compared the value with the reported Freight Tonnes Kilometer (FTK) for 2018, i.e., 17.5 trillion tonnes·km (Cargo Airports & Airline Services, 2019), obtaining an average load factor of 68% which is in line with the integrator's strategy (Aviation News, 2019).

Focusing on the *Cargolux sub-network*, most indices are aligned with the three integrators apart from reciprocity, which displays a considerably lower value. We believe the higher unidirectionality of connections is to be associated with the more hub-and-spoke oriented design of the *Cargolux sub-network*, where only LUX and MXP are hubs and, from a global perspective, behave as a single multiplex hub given their proximity. On the other hand, FedEx and UPS are multi-hub networks both within the United States and in Europe and Asia, with DHL being a hybrid between Cargolux and the other two integrators.

Finally, the *non-integrator sub-network* is the most developed, with an increase in density and reciprocity that reflects the substantial increase of bidirectional flows. This fact is also confirmed by the decrease in diameter with respect to the integrators and full-cargo sub-networks. Note that, although reciprocity increases because of passenger-oriented airlines, some connections will still be severely unbalanced because of the intrinsic directionality (and much greater capacity) of freighter services as opposed to passenger aircraft.

To conclude this preliminary topological analysis, we provide an overview of all the triangular routes that we identified in the *FedEx*, *UPS*, *DHL*, and *Cargolux sub-networks*. We decided to exclude the *non-integrator sub-network*, given the much higher reciprocity value. Note that, in this context, we define triangular routes as airport triplets that are connected by unidirectional routes only, thus forming a cycle. The concept of triangular route might be extended to airport triplets where one or two of the three connections are bidirectional or, with a slight abuse of notation, to cycles involving more than three airports. In this work, we only focused on triangular routes satisfying the definition provided above.

Fig. 5 shows the identified triangular routes. As expected, for the great majority of them at least one vertex is represented by a hub, which is a common practice in the cargo business for maintenance reasons. For FedEx, DHL, and Cargolux we identified routes passing through their main hubs, respectively MEM, CVG, and LUX. For UPS, we did not identify routes passing through the main hub SDF. On the other hand, routes through the national hubs DFW and PHL were highlighted. Examples of triangular routes are MEM-DXB-HKG, ANC-EWR-SEA, LGG-DXB-HKG (FedEx), CGN-PVG-ICN, DFW-PDX-PHX, DFW-PHL-LCK (UPS), CVG-BAH-HKG, CVG-HNL-HKG, HKG-LAX-HNL (DHL), and LUX-HKG-OVB, MXP-JKF-IAH, MXP-HKG-OVB (Cargolux). Interestingly, Cargolux was characterized by more triangular routes than FedEx and UPS, which is consistent with the lower reciprocity value of its sub-network. Note that we could relax our constraint on triangular routes (i) by allowing more than one transshipment option (i.e., switching from triangular to circular routes), and (ii) allowing connections forming the circle to be bi-directional, as long as some of them display a strong AFT imbalance. One example of such circular route is the UPS "around-the-world" route (UPS Pressroom, 2020) SDF-DXB-SZX-ANC,

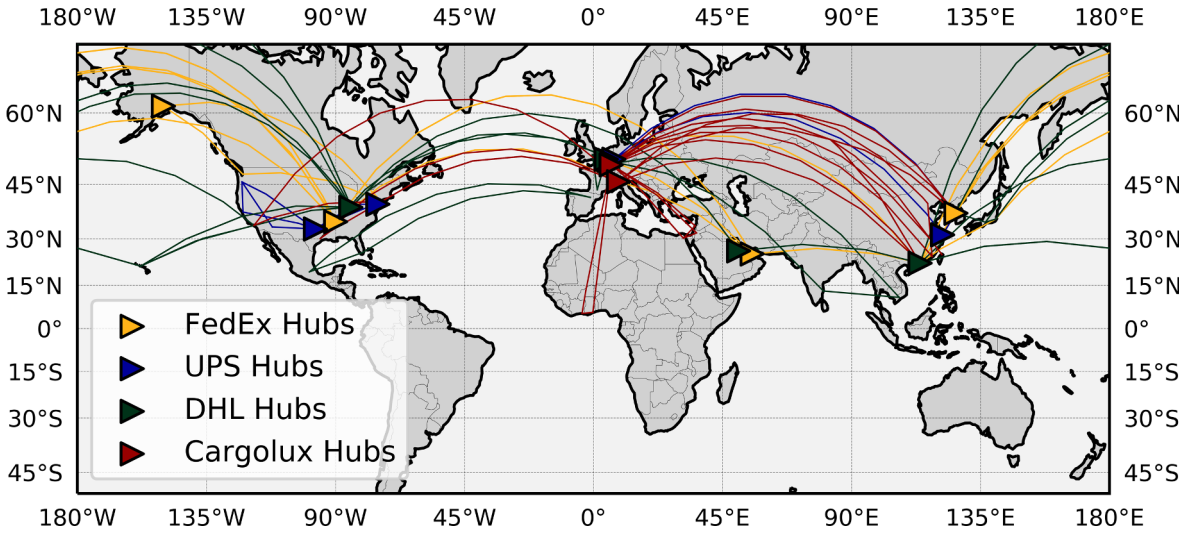

Fig. 5. Triangular routes in the ACTN.

where all four flight legs are bi-directional, but with a capacity ratio between the two directions of 57.0 (SDF-DXB), 6.5 (DXB-SZX), 3.5 (SZX-ANC), 1.8 (ANC-SDF), respectively.

5.2. Analysis of the global network

After the preliminary topological analysis that focused on sub-networks separately, we now focus our attention on the full ACTN, obtained as superimposition of the *FedEx*, *UPS*, *DHL*, *LATAM*, and *non-integrator sub-networks*. The ACTN is characterized by 335 airports with a yearly international cargo throughput above 5,000 tonnes, i.e., $|\mathcal{N}| = 335$. For the set of edges $\mathcal{E}$, we identified 7,574 directed routes, i.e., $|\mathcal{E}| = 7{,}574$. The ACTN is characterized by a density of 0.068 and a reciprocity of 0.77. The average degree of the ACTN is $\langle k \rangle = 45.2$. In addition, $\langle C \rangle = 0.53$ $|\mathcal{G}_c| = 335$ (i.e., the ACTN is its own giant component), $\langle L \rangle = 2.31$, and $D = 5$. According to closeness centrality, CDG is the closest airport in the ACTN, with a value of 0.644. This means that, on average, it takes at most one transshipment stop to go from CDG to any other airport, or vice versa, in the ACTN. The overall cumulative yearly AFT and AFTK (obtained summing the AFT and AFTK of all 7,574 directional edges in the network) are, respectively, 90,160,701 tonnes and 395,285,957,596 tonnes·km.

To provide more insights on the asymmetry of the directed network, we isolated the 3,284 $\mathcal{OD}$ airport pairs that are served in both directions, with the remaining 1,006 displaying unidirectional flows. Hence, the percentage of $\mathcal{OD}$ airport pairs that are served in both directions and in a single direction are, respectively, 77 and 23%, in accordance with the reciprocity value. This asymmetry, which is more significant than the average asymmetry of the air passenger traffic network (Verma et al., 2014), could be explained by the presence of more triangular and circular routes in the air cargo network due to imbalances in the demand flow and maintenance reasons (full freighters need to rotate to undergo checks in maintenance hubs at fixed intervals). This places the ACTN in an intermediate position between the WAN (Guimera and Amaral, 2004), where asymmetry was deemed to be negligible, and the GCSN (Kaluza et al., 2010), where only 41% of $\mathcal{OD}$ port pairs were connected in both directions.

For the $\mathcal{OD}$ airport pairs where connections in both directions exist, we compared the two yearly AFT as shown in Fig. 6. While directed trade flows are reasonably balanced for yearly AFT below 2,000 tonnes, non negligible imbalances are present otherwise. We identified the most imbalanced $\mathcal{OD}$ airport pairs by computing the absolute value of the difference of AFT in the two directions, and sorting results in descending orders. The ten most imbalanced airport pairs are ICN-ANC, HKG-ANC, PVG-ANC, SIN-BKK, ANC-SDF, ANC-CVG, ICN-HKG, NBO-AMS, NRT-ICN, NRT-TPE (where the order of airports represents the direction with the highest yearly AFT). Most connections are from North Eastern Asia to ANC, and represent the strong high-tech export from Asia towards the United States using ANC as pivot airport. To further strengthen the identification of this pattern, other highly imbalanced connections are ANC-SDF and ANC-CVG, which identify the second leg for the high-tech import flow for integrators UPS and DHL, respectively. Focusing on a completely different commodity, a noticeable imbalance is NBO-AMS, with a yearly AFT of 115,559 versus 15,912 in the other direction, caused by the flower trade from Kenya to the Netherlands. We identified 140 $\mathcal{OD}$ airport pairs where the imbalance between the AFT in the two directions exceeds 20,000 tonnes. For comparison purposes, this is the cumulative weight capacity of over 142 Boeing 747-800F, one of the biggest full freighter currently existing.

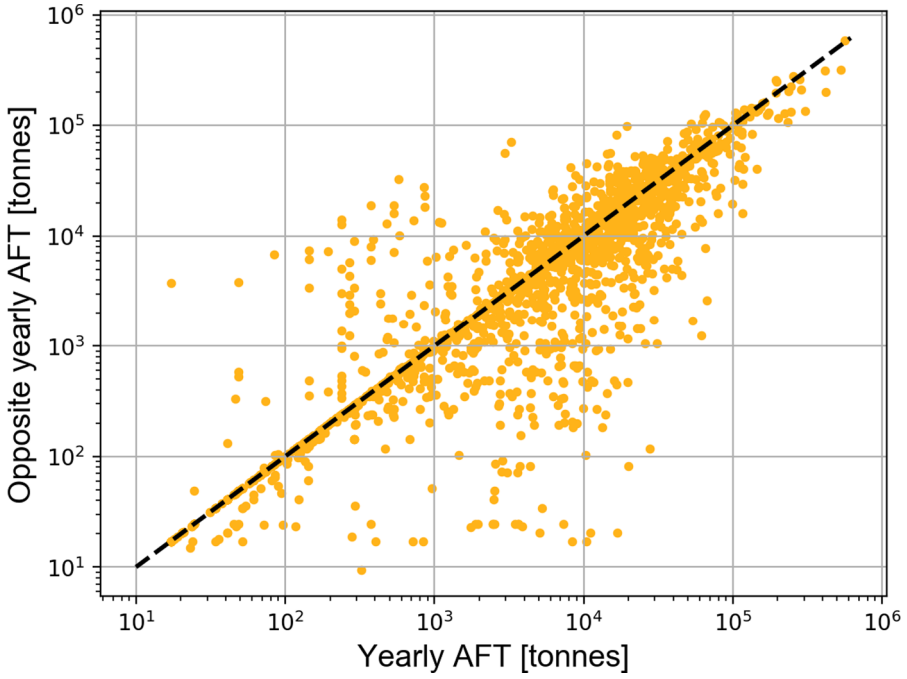

Fig. 6. Comparison between yearly AFT for $\mathcal{OD}$ airport pairs served in both directions (logarithmic scale).

In the full ACTN, we identified 53 triangular routes that are a combination of routes flown by the three integrators and by full-cargo airlines. We noticed that some of the triangular routes that were identified in Fig. 5 did not appear any longer because of the presence of the *non-integrator sub-network* and its wider net of connections. In particular, triangular routes passing through cargo hubs that are also hubs from a passenger perspective (e.g., DXB and HKG) generally lost their triangularity feature in the full ACTN. On the other hand, triangular routes relying on airports that are hubs only from a cargo perspective (e.g., ANC, CVG, and LUX) retained their triangularity feature in the full ACTN. Among the 53 triangular routes, we also identified some new routes with respect to Fig. 5 to be attributed to other full-cargo airlines or passenger airlines with a consolidated cargo orientation. Examples of such routes are ANC-MIA-ATL, BOM-CGN-PVG, and IST-KRT-NBO.

To get a better overview of the yearly cargo capacity of the ACTN, we sorted $\mathcal{OD}$ airport pairs by yearly AFT decreasing order. The top five connections are TPE-HKG, HKG-TPE, HKG-ANC, ICN-ANC, ICN-HKG, with a yearly AFT of 583,324, 560,885, 530,067, 419,033, 416,266 respectively. We also estimated the daily cargo capacity by dividing the yearly capacity by 365 days, obtaining a value of 247,043 AFT/day. We compared this value with (IATA, 2020a), where it is stated that on average, 140,000 tonnes of cargo are transported on a daily basis. The ratio between the two values is 0.57, which can be interpreted as an average global load factor. In the air cargo industry, load factors might exhibit variations both by airline and by region. As example, Cargolux reported a load factor of 67.9% in 2018 (Cargolux, 2019), LATAM reported a load factor of 55.2% for the same year (LATAM, 2019), while Singapore Airlines Cargo reported a value of 58.1% for January 2019 (AirCargoNews, 2019). Similarly, load factors in December 2014 exhibited variations according to the specific continent (PlaneStats, 2019). We acknowledge that, provided data availability, the best approach is to replace yearly estimated AFT with actual flown tonnes. This would automatically include differences in load factors across different airlines and across different geographic areas, by providing a direct comparison between the flown tonnes and the maximum capacity per $\mathcal{OD}$ airport pair.

Notwithstanding the load factor variations, and facing the issue of data unavailability when it comes to actual flown cargo tonnes, we believe that our approach, based on estimated yearly AFT to characterize $\mathcal{OD}$ airport connections, provides a good foundation for a complex network analysis of the ACTN. In addition, our average global load factor of 57% well compares with the average load factors of some major full-cargo airlines, and with regional data referring to the Asia/Pacific region (PlaneStats, 2019).

To assess the relevance of centrality indicators in the ACTN, we computed some indices that are either node- or edge-specific and ranked them by decreasing order. The indices are (i) degree, (ii) strength, (iii) modal contribution, (iv) betweenness centrality and (v) betweenness edge centrality. For the two betweenness measures, we weighted edges using three approaches: (1) unweighted approach, (2) distance-weighted approach, (3) capacity-weighted approach. Approaches (1) and (2) did not require any manipulation. In fact, in both cases edges are already characterized by a cost and the triangular inequality is satisfied. In this work, the shortest path between two airports is always the direct connection, if such connection exists. This reflects the preference of freight forwarders towards direct shipping lines to avoid delays at transshipment airports, even if direct connections are generally more expensive (Boonekamp and Burghouwt, 2017). In fact, satisfying delivery time windows is of paramount importance for freight forwarders, given that time windows are agreed with shippers as part of the contract, and minimizing the number of transshipment options reduces possible sources of delays.

For approach (3), we used estimated AFT to characterize each edge. According to the definition provided in Section 3, AFT are strengths rather than costs. Hence, when computing betweenness centrality, we used a two-stage approach. In the first stage, we determined whether the current $\mathcal{OD}$ airport pair had a straight connection. If so, the straight connection was assumed to be the shortest path, to reflect the aforementioned shipping preference. If not, in the second step a K-shortest path algorithm (Yen, 1970) was used assuming unweighted edges, in order to identify paths with the minimum number of transshipment options. To limit the computational burden, we set $K = 15$. Among the subset of routes with the smallest number of steps, we selected the one with the highest average AFT among the different flight legs, i.e., the route with the highest (on average) cargo capacity. If we would use, as example, the inverse of each AFT to define the cost of an edge, we might have the undesirable effect to compute shortest paths that are sequences of high-capacity connections, rather than a low-capacity direct connection. Our two-stage approach mitigates this effect. In addition, we do not consider congestion in our betweenness measure. This means that, as example, a certain airport might appear in a set of shortest paths whose cumulative supply level exceeds the processing capabilities of such airport. This is an intrinsic limitation of every betweenness centrality measure which we did not address in this work.

For edge betweenness indices, we imposed a lower bound on both the available AFT per connection, and the distance between airports. The bounds are 20,000 tonnes and 300 km respectively. The choice was carried out to filter out connections that might appear in the unweighted or distance-weighted formulation, but whose relevance in the air cargo network is not corroborated by a sufficient capacity level. Note that the two bounds are strongly inter-related. Generally speaking, airports that are easily connected via RFS only have a limited available air transport capacity, and heavily rely on ground transportation if shipments need to moved (Boonekamp and Burghouwt, 2017).

The ten highest-ranked airports according to the different node-based and edge-based indices are reported in Table 4 and Table 5, respectively. The airports with the highest number of connections are all major hubs both from a passenger and a cargo perspective, as Table 4 highlights. They are geographically divided between Europe, Northeast Asia, and the Middle East. Strength and modal contribution identify the role of major transshipment airports (e.g., ANC, DXB, ICN, NRT), or of integrator hubs (MEM and SDF). The transshipment-oriented role of DXB, where 85% of the flow (Emirates, 2018) is transshipped, is highlighted by all betweenness centrality measures, which all rank the airport in the top three positions. Comparing the three betweenness centrality definitions, we generally noticed a strong consistency between the approaches. On the other hand, ANC is a top-ten airports only when cargo capacity is explicitly considered. ANC is an airport which relies on a relatively low number of connections characterized by a high maximum capacity, and thus its relevance is not fully revealed by g and g_d.

Table 4
Highest-ranked airports according to degree k, strength s, modal contribution w, unweighted betweenness g, distance-weighted betweenness g_d, and capacity-weighted betweenness g_c.

	k		s [tonnes·1e6]		w [tonnes·1e6]		g		g_d		g_c	
Rank	Airport	Value	Airport	Value	Airport	Value	Airport	Value	Airport	Value	Airport	Value
1	CDG	302	HKG	10.20	ICN	9.13	CDG	0.12	CDG	0.07	DXB	0.12
2	DXB	293	ICN	6.06	NRT	8.39	DXB	0.09	MIA	0.06	CDG	0.11
3	FRA	263	PVG	5.28	HKG	8.37	FRA	0.07	DXB	0.06	AMS	0.11
4	HKG	220	MEM	5.05	PVG	8.08	MIA	0.06	ICN	0.05	HKG	0.10
5	LHR	213	DXB	4.89	ANC	7.95	HKG	0.06	IST	0.05	BKK	0.10
6	AMS	210	TPE	4.80	TPE	7.64	AMS	0.05	HKG	0.05	FRA	0.08
7	IST	203	NRT	4.59	BKK	6.14	JKF	0.04	AMS	0.05	MIA	0.07
8	JKF	201	ANC	4.32	SIN	5.90	MAD	0.03	FRA	0.05	ANC	0.05
9	DOH	198	SIN	4.21	MEM	5.74	IST	0.03	JFK	0.05	ICN	0.04
10	ICN	191	SDF	3.99	MIA	5.23	LEJ	0.03	PEK	0.03	JFK	0.03

Table 5
Highest-ranked airport connections according to unweighted edge betweenness g_e, distance-weighted edge betweenness $g_{e,d}$, and capacity-weighted edge betweenness $g_{e,c}$.

	g_e		$g_{e,d}$		$g_{e,c}$	
Rank	Connection	Value	Connection	Value	Connection	Value
1	UIO-MIA	0.0023	PEK-ICN	0.0018	AMS-MIA	0.0201
2	MIA-AMS	0.0016	MEM-MIA	0.0017	AUH-AMS	0.0120
3	SDF-DXB	0.0016	MIA-MEM	0.0016	AMS-BKK	0.0116
4	AMS-MIA	0.0015	CGN-EMA	0.0012	AMS-DXB	0.0098
5	LHR-MIA	0.0013	ICN-TPE	0.0012	CDG-DXB	0.0094
6	PEN-HKG	0.0012	ANC-MEM	0.0011	ATL-CDG	0.0091
7	CDG-NRT	0.0011	HKG-TPE	0.0011	MIA-AMS	0.0083
8	CDG-MEM	0.0011	HKG-DXB	0.0011	HKG-ANC	0.0080
9	HKG-LEJ	0.0011	MIA-AMS	0.0118	ANC-SDF	0.0061
10	MIA-LHR	0.0010	SDF-ORD	0.0010	CDG-MEM	0.0052

Focusing on edge betweenness centrality, the unweighted, distance-weighted, and capacity-weighted approaches display a higher degree of variation with respect to node betweenness centrality. Notwithstanding the higher variation, some common patterns can still be identified. The strategic location of MIA is highlighted both all indices, especially by g_e and $g_{e,d}$. Connections to South America, North America and Europe testify the relevance of the airport as a transshipment hub for cargo flows from/to the aforementioned trade regions. The role of integrator hubs MEM, SDF, ANC, CDG, EMA, LEJ is also revealed by the indices. Focusing on $g_{e,c}$, the role of the two top European airports, CDG and AMS, is highlighted, mainly thanks to the combination of the density of airports in Europe (i.e., richness of shortest paths) and high capacity levels per connection. Additionally, it could be noted how the connections where ANC appears follow the West-to-East direction that characterizes most of integrators' routes. In particular, it is caught the capacity imbalance from Asia to Anchorage (HKG-ANC), and from Anchorage to integrator hubs (ANC-MEM, ANC-SDF) that is consistent with "around-the-world" routes. Removing the directionality modeling assumption from the ACTN, this behavior would be lost.

Having the values of $\langle L \rangle$ and D in mind, we also assessed the shortest path distribution in the ACTN, which is summarized in Table 6. More than 98% of all $O\mathcal{D}$ airport pairs are characterized by, at most, two transshipment stopovers, with a single stopover being the most common routing option.

$\langle L \rangle$ is considerably smaller than the one characterizing the WAN (Guimera and Amaral, 2004), and very similar to one characterizing the GCSN (Kaluza et al., 2010). This suggests that cargo networks, that rely on RFS as part of their logistic chain, are more concentrated with a lower characteristic length. In addition, recalling the definitions provided in Section 3, the $\langle L \rangle$ and $\langle C \rangle$ values

Table 6
Distribution of shortest path lengths in the ACTN.

Steps	$\lvert O\mathcal{D} \rvert$	% $O\mathcal{D}$
1	7574	6.76
2	64,030	57.23
3	38,478	34.38
4	1782	1.63
5	26	0.02

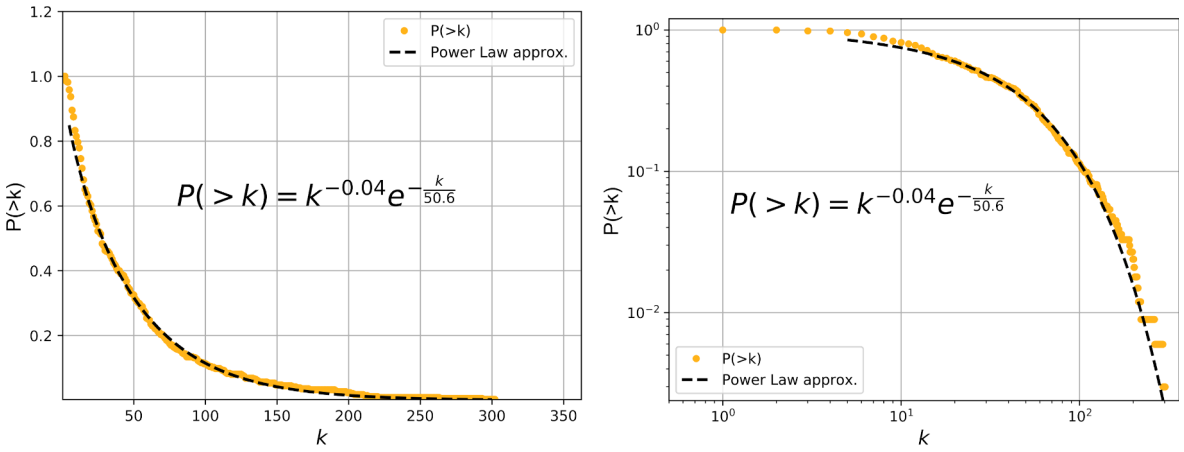

(a) Linear scale. (b) Logarithmic scale.

Fig. 7. Cumulative degree distribution $P(>k)$ for the ACTN.

suggest the ACTN is a typical small-world network (Barrat and Weigt, 2000).

$P(>k)$ was also computed to assess if the ACTN had scale-free characteristics. In passenger air transport networks (Guimera et al., 2005; Verma et al., 2014) $P(>k)$ was shown to follow a truncated power law, i.e., $P(K>k) \sim k^{-\gamma}\exp\left(-\frac{k}{k_x}\right)$, hence exhibiting scale-free characteristics. This is a common feature among transportation networks associated with different modes (rail, subway, air transportation), although recent studies are highlighting that a strongly scale-free structure is empirically rare (Broido and Clauset, 2019). In particular, in Guimera et al. (2005) it was reported $\gamma = 1.0 \pm 0.1$, while in Verma et al. (2014) it is shown that $\gamma = 1.5 \pm 0.1$ and $k_x \approx 180$. In Fig. 7 we show the cumulative degree distribution, as well as the truncated power law that best approximates the distribution. The parameters of the function are $\gamma = 0.04$, and $k_x = 50.6$. We noticed that the power law exponent is considerably smaller than the one in Guimera et al. (2005) and Verma et al. (2014). For low values of k (e.g., $1 \leqslant k \leqslant 10$), $P(>k)$ decreases less steeply than its WAN counterpart, which means that the decrease in the cumulative probability is less pronounced in the ACTN (i.e., in proportion, a higher percentage of airports with a low degree is present in the WAN). On the other hand, the ACTN differs from the ATNC (Wang et al., 2011), whose cumulative degree distribution was shown to follow an exponential curve. Given that $P(K>k)$ follows a truncated power law, the ACTN is also a scale-free network.

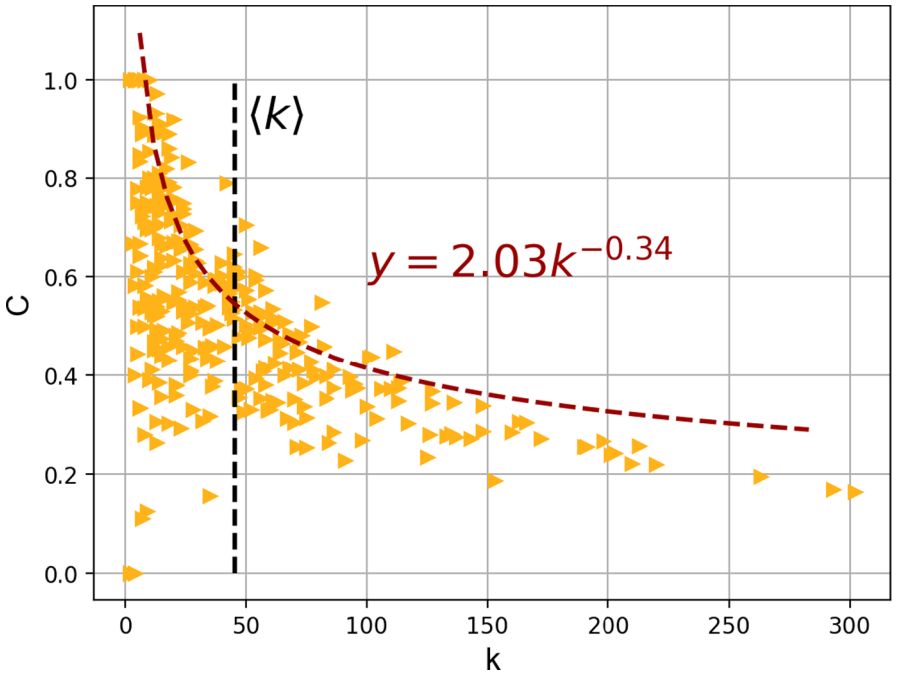

Fig. 8. Comparison between degree k and local clustering coefficient C for the ACTN.

We also compared the degree and the local clustering coefficient C. In Fig. 8, the degree and local clustering coefficient are plotted for the 335 airports forming the ACTN. C is by definition zero for all airports with a unitary degree, while for airports with a low degree (i.e., $k \leqslant 10$), C ranges from zero to a unitary value. This situation represents the case of small communities of local cargo airports that are generally all connected. As k increases, we noticed a decrease in C that is particularly evident for airports with $k \geqslant 20$. The C curve is monotonically decreasing, with the most connected airport according to k, i.e., CDG, characterized by the lowest local clustering coefficient among this set of airports. The shape is similar to the inverted-V shape that was found in Wang et al. (2011), with two differences. First, the change in slope occurs before, and not in correspondence to $\langle k \rangle$, and second, in our case the right branch has a more pronounced concavity. Both differences suggest a more hub-and-spoke oriented layout, where second-tier airports are connected to the main hub, but not necessarily among each other. This further justifies the assumption that the ACTN is characterized by more concentrated flows than a passenger counterpart. In Fig. 8, we also plot $\langle k \rangle$ and the best power law fit $y = ak^b$ (with $a = 2.03$ and $b = -0.34$) of the right branch boundary of the k-C distribution.

6. Airport relevance in the air cargo transport network

In Section 5, a thorough analysis of the topology of the ACTN was provided. What the section did not fully reveal, as example, is to what extent a disruption of an airport that is highly ranked for degree, compare with a disruption of an airport highly ranked for betweenness. In other words, we now want to understand if airports considered crucial according to different indices, play a similar or a different role in the connectivity of the ACTN.

We followed an approach similar to Lordan et al. (2014), simulating attacks resulting in the removal of an airport. This attack simulates the complete shutdown, or an extremely severe disruption, of an airport. Natural hazards, such as the eruption of the Eyjafallajökull volcano in 2010, but also national strikes (IAR, 2019) can cause this type of disruptions. We recursively remove from the network the airport with the highest value of the index under scrutiny, and use the size of the giant component of the updated network as robustness measure. For sake of clarity, in every analysis we plotted the normalized size of the giant component as a function of the ratio of removed airports $S(q)$, obtained dividing the size of the actual giant component by $|\mathcal{N}|$, i.e., $S(q) = |\mathcal{G}_c(q)|/|\mathcal{N}|$. We compared five removal strategies based on (i) degree k, (ii) strength s, (iii) modal contribution w, (iv) capacity-weighted betweenness centrality q_c, and (v) random node removal. For removal strategy (v), we averaged the outcome of 500 statistically independent cases, where airports were sequentially removed at random.

Fig. 9(a) shows, for the five removal strategies, how the size of the giant component $S(q)$ decreases as a function of the ratio q of the removed nodes. To complement the analysis, in Fig. 9b) and and Fig. 9(c) we respectively report the evolution of $\langle L \rangle$ and $\langle k \rangle$. The random removal strategy shows a linear relationship between q and $S(q)$ that can be approximated with the expression $S(q) = -q + 1$. As intuition would suggest, it is the least effective attack strategy. The other four strategies display a similar behavior until $q = 0.15$. After this value, attacks targeting q_c and k have a more disruptive effect in reducing the size of the giant component. Capacity-weighted betweenness is the index which causes the steepest drop because it removes transshipment-oriented airports first, which frequently appear in shortest paths, thus isolating the ACTN into communities. From Fig. 9(b), the different effect on the ACTN of attacks targeting k and g_c is evident. In fact, attacks based on k mainly affect connectivity within different hub-and-spoke communities by removing the hub. As a consequence, second-tier airports (the spokes) will experience a increase in $\langle L \rangle$ because they lose their pivot airport. Attacks based on g_c, as already introduced, tend to isolate communities because they remove bridges between communities instead. While the decrease in $S(q)$ is generally more pronounced, connectivity properties within the surviving biggest community are preserved. While attacks focused on k tend to destroy intra-community connectivity (as testified by the sudden growth in $\langle L \rangle$), attacks focused on g_c tend to destroy bridges between communities, hence affecting inter-community connectivity, before weakening connectivity within communities. As a consequence, apart from a spike for $q \approx 0.28$, the characteristic path length for attacks based on capacity-weighted betweenness is smaller than the ones characterizing attacks based on degree. Consistently, the drop in $\langle k \rangle$ is more pronounced for attacks targeting the degree, as shown in Fig. 9(c).

In Fig. 10, we report a visual interpretation of this different behavior using an example with three hub-and-spoke communities, and a node behaving as bridge between communities. The removal of a hub (red circle) would increase the average characteristic length within the associated community, without severely jeopardizing inter-community properties and the size of the giant component. On the other hand, the removal of a bridge airport (green circle) would disintegrate the network by isolating the right hub-and-spoke community, while leaving intact connectivity properties of the resulting giant component (two hub-and-spoke communities on the left). For removal strategies (i)-(iv), in Table 7 are listed the top ten ranked airports that were sequentially removed. The crucial role of integrator hubs ANC, MEM, and SDF is only highlighted by those indices (s, w, and g_c) that explicitly consider available capacity. Only modal analysis and capacity-weighted betweenness highlights the importance of both NRT and ANC as transshipment stops. As example, strength does not highlight ANC, while modal analysis does. The latter index better catches the repercussions on the global network (recall the structural analogy from Section 3) deriving from the removal of the airport and its bridge-like properties.

To corroborate our previous statement, we provide an additional analysis on the effect of the removal of a bridge airport like ANC from the network. More specifically, we analyzed the export cargo flow from China to the United States. For each of the 20 Chinese airports in the ACTN, we computed the shortest path to each of the 43 (ANC excluded) airports located in the United States. In 24% of the paths, ANC appears as a transshipment option, with a characteristic path length for the 860 $\mathcal{OD}$ airport pairs considered of 2.73. We then removed ANC from the network, and computed again the shortest paths. We noticed that the characteristic path length was almost unchanged, which is consistent with the structure of the ACTN. In fact, differently from the network represented in Fig. 10, communities are more densely connected to each other and can rely on more than a single bridge airport for inter-community

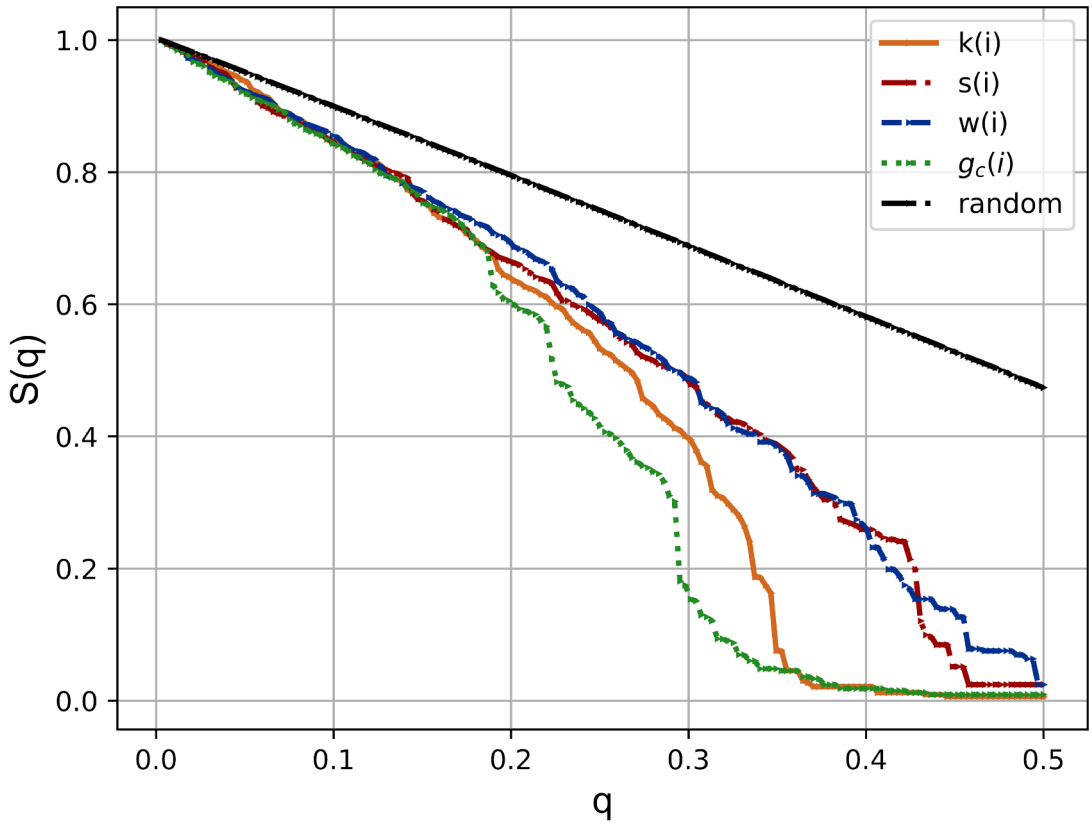

(a) $S(q)$.

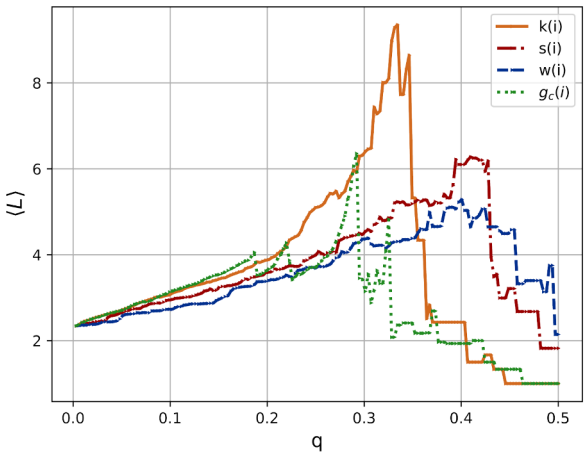

(b) $\langle L \rangle$.

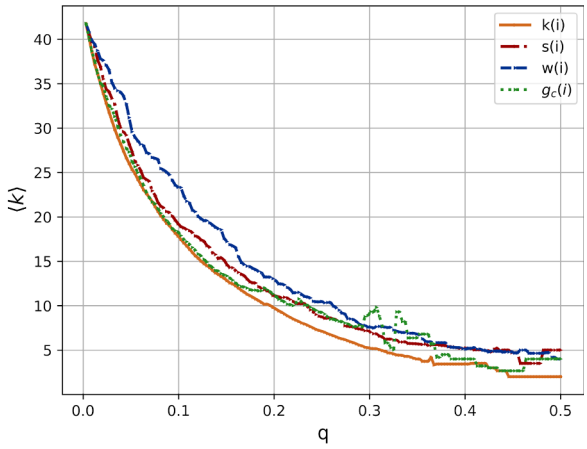

(c) $\langle k \rangle$.

Fig. 9. Evolution of $S(q)$, $\langle L \rangle$, and $\langle k \rangle$ as a function of the ratio of removed airports q for different attack strategies.

transport. Hence, the removal of ANC does not sensibly increase the number of transshipment options to fly from China to the United States. On the other hand, we experienced a considerable drop in the average AFT per route, as shown in Fig. 11.

For the 203 routes affected by the ANC removal, we computed an average decrease in available capacity of 71.5%. Apart from UPS and DHL main hubs SDF and CVG, respectively, the drop in available capacity was particularly evident in national cargo hubs such as DFW, OAK, ONT, and ORD, with some routes experiencing up to 90% in capacity reduction. The striking dichotomy between the variation in characteristic path length and available capacity before and after the removal of ANC, testifies the bottleneck role, for high-capacity trade flows, of the airport. While equivalent options (in terms of number of flight legs) exist, none of them is capable of accommodating the same demand level as the original itinerary passing through ANC.

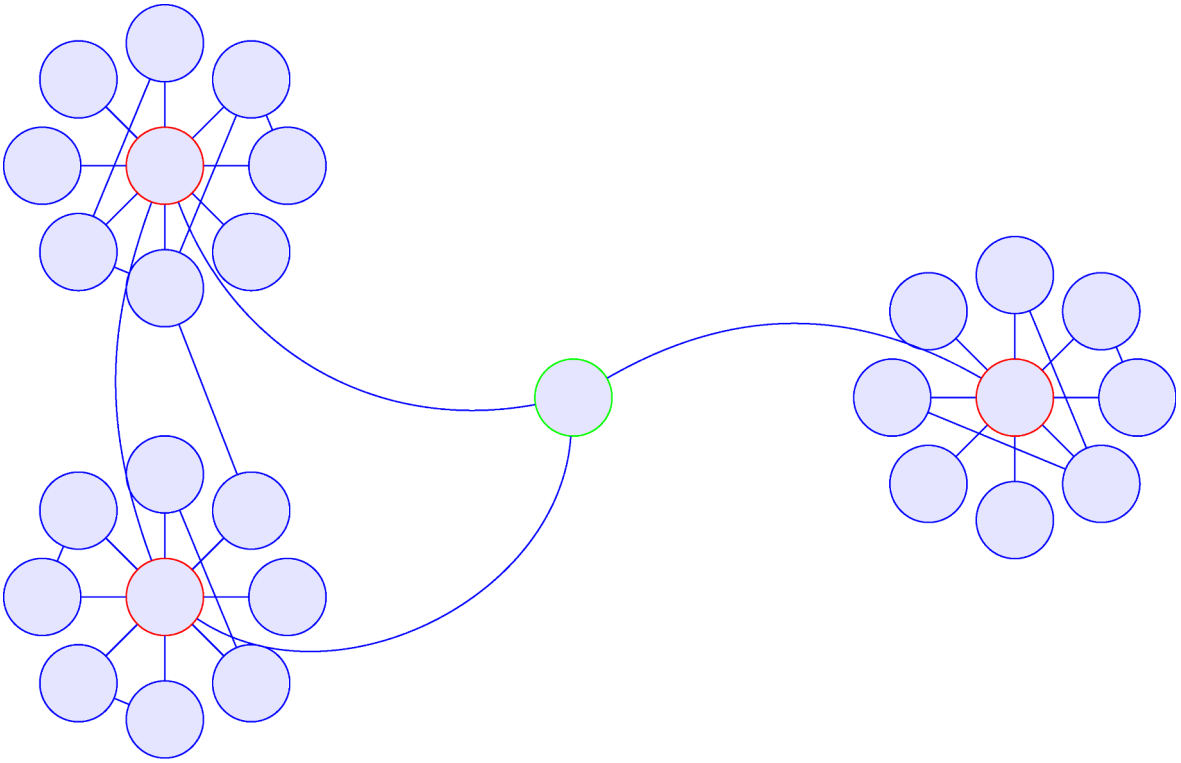

(a) Original network.

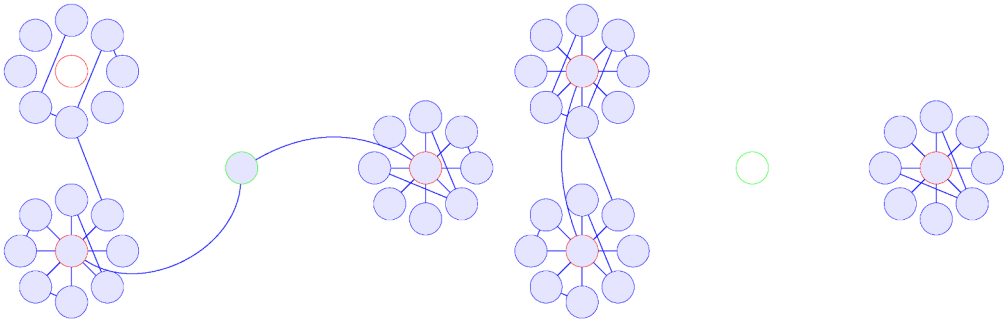

(b) Removal of hub airport. (c) Removal of bridge airport.

Fig. 10. Example of the effect of the removal of hub or bridge airport on a network.

Table 7
Highest-ranked airports for attack strategies based on k, s, w, and g_c.

Rank	k	s	w	g_c
1	CDG	HKG	ICN	DXB
2	DXB	ICN	NRT	CDG
3	FRA	MEM	ANC	HKG
4	HKG	DXB	TPE	ANC
5	LHR	PVG	PVG	FRA
6	AMS	FRA	HKG	AMS
7	IST	LHR	MEM	MIA
8	DOH	SDF	MIA	LHR
9	BKK	NRT	FRA	ICN
10	ICN	SIN	SIN	NRT

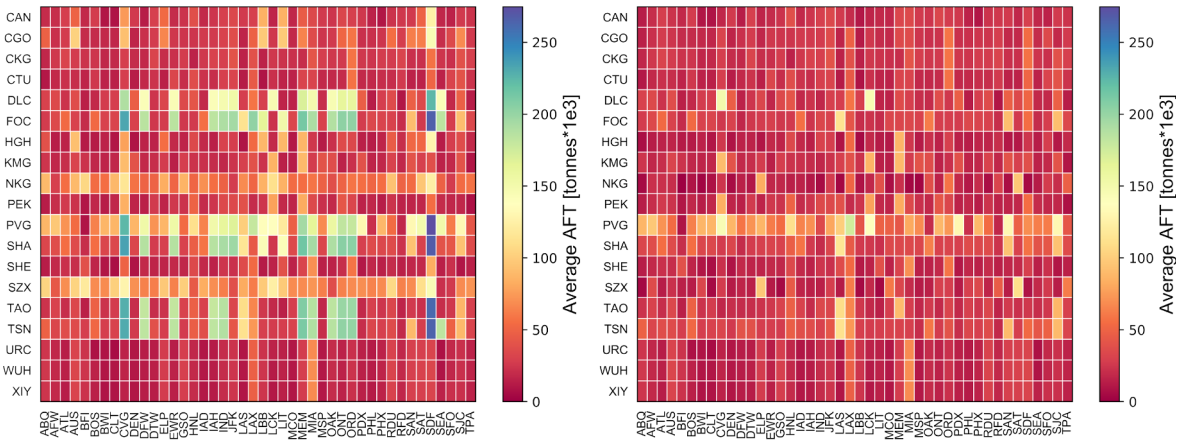

(a) With ANC. (b) Without ANC.

Fig. 11. Average yearly AFT per route from China to the United States.

7. Conclusions

In this paper, the Air Cargo Transport Network (ACTN) has been presented and analyzed from a complex network theory perspective. Our major findings are summarized and critically discussed as follows.

The ACTN presents unique topological features that are different than its passenger counterparts. Similarly to passenger air transport networks, the ACTN is both a small-world and a scale-free network. In fact (i) it is characterized by a small $\langle L \rangle$ and a large $\langle C \rangle$, and (ii) its cumulative degree distribution follows a truncated power law. Differently from its passenger counterparts, the power law is more flat for low degree values, highlighting the scarcer peripheral layer that characterizes the ACTN. This difference highlights the higher concentration and more hub-oriented routing of the air cargo with respect to the passenger network. This is also confirmed by the smaller values of $\langle L \rangle$ and D, and the larger value of $\langle k \rangle$ (accounting for the directionality) when compared to passenger air transportation networks.

We computed the reciprocity value of the ACTN, expressed as ratio between $O\mathcal{D}$ airport pairs with connections in both directions and $O\mathcal{D}$ airport pairs with connections in at least a direction. This resulted in a value that is higher than the same indicator for integrators or full-cargo airlines networks because of the presence of passenger airlines offering cargo services and their more extensive network. When assessing imbalances in the directionality of cargo capacity, the ACTN showed a major difference with respect to its passenger counterpart. Although many connections might be reciprocal, capacities are highly imbalanced because of the presence of triangular and circular routes that are not part of passenger air transport systems. This fostered our modeling choice to consider the ACTN as a directed graph.

When assessing the topological properties of the ACTN, we noticed that centrality measures do not univocally determine the relevance of airports in the network. In particular, the role of major transshipment hubs that rely on a low number of high-capacity connections might be missed if the capacity of those connections is not explicitly considered. Consistently with the cumulative degree distribution, we noticed that the ACTN is characterized by a peripheral layer that is dramatically scarcer than in passenger air transport networks because it does not account for local airports serving tourism-oriented or remote regions. In the air cargo business, the airport catchment area is much larger than for passengers, because it relies on Road Feeder Services for the ground leg that are not present in passenger networks.

We highlighted how (i) airports that are hubs of hub-and-spoke communities, and (ii) airports that operate as bridges connecting communities play a very different role in the overall ACTN. We also showed that removing transshipment-oriented airports such as ANC might not have a disruptive effect on the connectivity of the network (e.g., the characteristic path length is almost unaffected). On the other hand, the alternative routes are characterized by a much lower capacity level, and this might pose a serious threat, especially during peak periods, if bridge airports do not operate smoothly.

To the best of our knowledge, this is the first work that explicitly studies the air cargo network adopting a complex network theory perspective. As such, it could be extended in many ways. Provided the availability of actual flown cargo data, it would be interesting to provide a better characterization of airline-specific networks, to infer similarities and differences in network (and business) strategies. This is particularly relevant in an era where new key players, such as Amazon Air, have joined the air cargo business, to understand if and to what extent complex network indices can help airlines assess competition and network re-design opportunities. Another interesting research direction would be the comparison of global databases that are temporally spaced, using our global non-integrator database from 2014, and having access to a similar recent database (e.g, 2019). We could assess if there are tangible changes in the network topology due to the rise of some aircraft (e.g., Boeing 777 freighter), and the decline of others (e.g., passenger versions of Boeing 747), given the subsequent possibility to rely on ultra-long-flights and skip transshipment stops (e.g., the Monday-through-Saturday nonstop FedEx connection from Shanghai to Memphis).

CRediT authorship contribution statement

Alessandro Bombelli: Conceptualization, Methodology, Data curation, Formal analysis, Writing - original draft, Writing - review & editing. **Bruno F. Santos:** Conceptualization, Methodology, Writing - review & editing. **Lóránt Tavasszy:** Conceptualization, Methodology, Writing - review & editing.

Declaration of Competing Interest

The authors declare that they have no known competing financial interests or personal relationships that could have appeared to influence the work reported in this paper.

Acknowledgments

The authors would like to thank *Seabury Consulting* for sharing their dataset and making it available for this research. In addition, the authors would like to thank the editor and three anonymous reviewers for their careful comments, which improved the overall quality of this paper.

Appendix A. Cargo tonnage of different aircraft

In Table 8, we report the list aircraft types, together with the aircraft code, the transportable cargo tonnage, and the original source that was used to determine the cargo tonnage. For full freighters, the specified payload value was directly used given the absence of passenger payload. For some passenger aircraft, the maximum transportable cargo tonnage was explicitly specified. When this data was not available, we used the following approach.

Table 8
Cargo tonnage for different aircraft types.

Aircraft type	Code	Tonnage [tonnes]	Source
Airbus A300-600	A306	13.5	https://www.airbus.com/content/dam/corporate-topics/publications/backgrounders/techdata/aircraft_characteristics/Airbus-Commercial-Aircraft-AC-A300-600-Dec-2009.pdf
Airbus A300-600RF	A306RF	48	https://www.airbus.com/aircraft/previous-generation-aircraft/a300-600/a300-600f.html
Airbus A300-B2/B4	A300B2	12.7	https://www.airliners.net/aircraft-data/airbus-a300b2b4/17
Airbus A300-B4F	A300B4F	43.5	https://www.aircharterservice.com/aircraft-guide/cargo/airbuseurope/airbusa300b4f
Airbus A310-300	A313	12.5	https://www.airbus.com/content/dam/corporate-topics/publications/backgrounders/techdata/aircraft_characteristics/Airbus-Commercial-Aircraft-AC-A310-Dec-2009.pdf
Airbus A310-300F	A313F	39	https://www.aircharterservice.com/aircraft-guide/cargo/airbuseurope/airbusa310-300f
Airbus A330-200	A332	17	https://publikationen.bibliothek.kit.edu/1000075507
Airbus A330-200F	A332F	70	https://www.airbus.com/aircraft/freighter/a330-200f.html#details
Airbus A330-300	A333	17	https://publikationen.bibliothek.kit.edu/1000075507
Airbus A340-200	A342	17	https://www.airbus.com/aircraft/previous-generation-aircraft/a340-family/a340-200.html#details
Airbus A340-300	A343	19	https://www.airbus.com/aircraft/previous-generation-aircraft/a340-family/a340-200.html
Airbus A340-500	A345	18	https://www.airbus.com/aircraft/previous-generation-aircraft/a340-family/a340-500.html
Airbus A340-600	A346	25	https://www.airbus.com/aircraft/previous-generation-aircraft/a340-family/a340-600.html
Airbus A380-800	A388	17	https://www.skycargo.com/fleet/air-fleet/
Boeing B737-400F	B734F	20.5	https://www.euascargo.com/en/useful-info/freighter-aircraft/boeing-b737-400f
Boeing B747-200F	B742F	111.5	https://www.aircharterserviceusa.com/aircraft-guide/cargo/boeing-usa/boeingb747-200f
Boeing B747-300	B743	21.5	http://www.boeing.com/resources/boeingdotcom/company/about_bca/startup/pdf/historical/747-100_-200_-300_-SP_passenger.pdf
Boeing B747-400	B744	20.5	http://www.boeing.com/resources/boeingdotcom/company/about_bca/startup/pdf/historical/747-400-passenger.pdf
Boeing B747-400F	B744F	112	http://www.boeing.com/resources/boeingdotcom/company/about_bca/startup/pdf/freighters/747-400f.pdf
Boeing B747-400 M	B744M	45	https://www.afklcargo.com/NL/en/common/about_us/boeing_747_400_combi.jsp
Boeing B747-8	B748	19.5	http://www.boeing.com/assets/pdf/commercial/airports/acaps/747_8.pdf
Boeing B747-8F	B748F	137	http://www.boeing.com/commercial/747/#/design-highlights/freighter/characteristics/
Boeing B747-SP	B747SP	13.5	http://www.boeing.com/assets/pdf/commercial/airports/acaps/747_123sp.pdf
Boeing 757-200F	B752F	35	https://www.boeing.com/resources/boeingdotcom/company/about_bca/startup/pdf/freighters/757f.pdf
Boeing B767-200	B762	13.4	http://www.boeing.com/assets/pdf/commercial/airports/acaps/767.pdf
Boeing B767-200SF	B762F	42.0	https://airlinesconnection.com/aircraft-charter/cargo-aircraft-charter/wide-body-freighters/boeing-b767-200sf
Boeing B767-300	B763	19.4	http://www.boeing.com/assets/pdf/commercial/airports/acaps/767.pdf

(*continued on next page*)

Table 8 (*continued*)

Aircraft type	Code	Tonnage [tonnes]	Source
Boeing B767-300ER	B763ER	19.4	http://www.boeing.com/assets/pdf/commercial/airports/acaps/767.pdf
Boeing B767-300ERF	B763ERF	58	http://www.boeing.com/farnborough2014/pdf/BCA/bck-767_5_13_2014.pdf
Boeing B767-400ER	B764ER	20.5	http://www.boeing.com/assets/pdf/commercial/airports/acaps/767.pdf
Boeing B777-200/200ER	B772	20.5	http://www.boeing.com/assets/pdf/commercial/airports/acaps/777_23.pdf
Boeing B777-200ER	B772ER	20.5	http://www.boeing.com/assets/pdf/commercial/airports/acaps/777_23.pdf
Boeing B777-200LR	B772LR	20.5	http://www.boeing.com/assets/pdf/commercial/airports/acaps/777_23.pdf
Boeing B777-200LRF	B772LRF	103	https://www.skycargo.com/fleet/air-fleet/
Boeing B777-300	B773	24.5	https://www.iagcargo.com/en/page/fleet/boeing-777-300
Boeing B777-300ER	B773ER	24	https://www.aircanada.com/cargo/en/shipping/fleet/#subtab_boeing777-300er
Boeing B787-8	B788	15.5	https://www.aircanada.com/cargo/en/shipping/fleet/#subtab_boeing787-8
Boeing B787-9	B789	16.5	https://www.aircanada.com/cargo/en/shipping/fleet/#subtab_boeing787-9
Boeing MD-11	MD11	19.5	http://www.boeing.com/resources/boeingdotcom/commercial/airports/acaps/md11.pdf
Boeing MD-11F	MD11F	91.9	http://www.boeing.com/resources/boeingdotcom/commercial/airports/acaps/md11.pdf, http://www.fedex.com/us/charters/md-11f.html
Ilyushin Il-96	IL96	25	https://en.wikipedia.org/wiki/Ilyushin_Il-96#Variants

If the maximum payload was specified, we computed the overall payload attributable to passengers following the guidelines we found in a EASA report on standard weights of passengers and baggage[3]. We used 91.3 kg and 72.5 kg for men and women, respectively, where the weight is inclusive of the carry-on luggage. We used an average weight of 19 kg for the luggage instead. We used a 70/30% split for men and women, and used the maximum number of passengers as suggested by the aircraft manuals.

If the maximum payload was not specified, we used the maximum number and type of ULDs that could be stored in the cargo area (we focused on container-only configurations), and multiplied that number by the maximum weight per ULD and by a correction coefficient to account for the simultaneous presence of luggage in the cargo area. We calibrated the correction coefficient using those passenger aircraft where the maximum cargo tonnage was specified, and found that a value $\in [0.35, 0.40]$ resulted in a good match between values.

Let us consider the example of the Boeing B777-300. Air Canada reports a cargo capacity of 24 tonnes. Using the first approach described above, we obtained $65 - 0.001 * 368(0.7 * 91.3 + 0.3 * 72.5 + 20) = 23.5$ tonnes. Using the second approach (it is reported that a maximum of 44 LD3 can be stored) we obtained $44 * 1.588 * 0.35 = 24.5$ tonnes. Although we believe the approach we proposed yields reasonable estimates for the cargo tonnage, we are aware that values might vary according to the specific aircraft configuration, airline, time of the year and specific flight: an exhaustive evaluation of cargo tonnage was beyond the scope of the paper. We also want to highlight how these differences might affect full freighters as well. As example, while Boeing reports a payload of 91.9 tonnes for the Boeing MD-11F, FedEx reports a value of 81.6 tonnes for the MD-11 aircraft part of its fleet[4].

References

ACI Blog, 2019. ACI blog website. https://blog.aci.aero/airport-markets-and-seasonal-variations/. Accessed: December 2019.

AirCargoNews, 2019. Air Cargo News website. https://www.aircargonews.net/airlines/sia-cargo-reports-disappointing-january-figures/. Accessed: September 2019.

AirCargoWorld, 2019. Air Cargo World website. https://aircargoworld.com/allposts/how-southwest-makes-low-cost-air-freight-work/. Accessed: September 2019.

Aviation News, 2019. Aviation News website. https://www.aviationnews-online.com/technology/ups-commits-to-14-747-8fs-and-orders-four-767f-iata-figures-fuel-optimism/. Accessed: December 2019.

Barabási, A.L., 2009. Scale-free networks: a decade and beyond. Science 325 (5939), 412–413.

Barabási, A.L., Albert, R., 1999. Emergence of scaling in random networks. Science 286 (5439), 509–512.

Barrat, A., Weigt, M., 2000. On the properties of small-world network models. Eur. Phys. J. B-Condens. Matter Complex Syst. 13 (3), 547–560.

Boonekamp, T., Burghouwt, G., 2017. Measuring connectivity in the air freight industry. J. Air Transp. Manage. 61, 81–94.

Bowen Jr, J., 2012. A spatial analysis of FedEx and UPS: hubs, spokes, and network structure. J. Transp. Geogr. 24, 419–431.

Brandes, U., 2001. A faster algorithm for betweenness centrality. J. Math. Sociol. 25 (2), 163–177.

Broido, A.D., Clauset, A., 2019. Scale-free networks are rare. Nat. Commun. 10 (1), 1017.

Burghouwt, G., Redondi, R., 2013. Connectivity in air transport networks: an assessment of models and applications. J. Transp. Econ. Policy 47 (1), 35–53.

Calatayud, A., Mangan, J., Palacin, R., 2017. Vulnerability of international freight flows to shipping network disruptions: A multiplex network perspective. Transp. Res. Part E: Logist. Transp. Rev. 108, 195–208.

Cardillo, A., Gómez-Gardenes, J., Zanin, M., Romance, M., Papo, D., Del Pozo, F., Boccaletti, S., 2013. Emergence of network features from multiplexity. Scient. Rep. 3, 1344.

Cardillo, A., Scellato, S., Latora, V., Porta, S., 2006. Structural properties of planar graphs of urban street patterns. Phys. Rev. E 73 (6), 066107.

Cargo Airports & Airline Services, 2019. Cargo Airports & Airline Services website. https://www.caasint.com/fedex-express-retains-top-spot-in-iata-wats-rankings/. Accessed: December 2019.

Cargolux, 2019. Cargolux website. https://www.cargolux.com/media-room/media-releases/media-releases/Cargolux-reaches-new-high-in-2018. Accessed: September 2019.

[3] https://www.easa.europa.eu/sites/default/files/dfu/Weight%20Survey%20R20090095%20Final.pdf

[4] http://www.fedex.com/us/charters/md-11f.html

Cohen, R., Erez, K., Ben-Avraham, D., Havlin, S., 2000. Resilience of the Internet to random breakdowns. Phys. Rev. Lett. 85 (21), 4626.
Crucitti, P., Latora, V., Porta, S., 2006. Centrality measures in spatial networks of urban streets. Phys. Rev. E 73 (3), 036125.
DC Velocity, 2020. DC Velocity website. https://www.dcvelocity.com/articles/20180412-ups-pilots-union-to-survey-large-shippers-to-determine-if-capacity-shortfalls-hurt-service/. Accessed: January 2020.
Du, W.B., Zhou, X.L., Lordan, O., Wang, Z., Zhao, C., Zhu, Y.B., 2016. Analysis of the Chinese Airline Network as multi-layer networks. Transp. Res. Part E: Logist. Transp. Rev. 89, 108–116.
Ducruet, C., Lee, S.W., Ng, A.K.Y., 2010. Centrality and vulnerability in liner shipping networks: revisiting the Northeast Asian port hierarchy. Maritime Policy Manage. 37 (1), 17–36.
Ducruet, C., Notteboom, T., 2012. The worldwide maritime network of container shipping: spatial structure and regional dynamics. Glob. Netw. 12 (3), 395–423.
Emirates, 2018. Emirates skycargo website. http://www.skycargo.com/english/Images/EKSC_A5_EventBrochure_new.pdf. Accessed: May 2019.
Fagiolo, G., 2007. Clustering in complex directed networks. Phys. Rev. E 76 (2), 026107.
Freeman, L.C., 1977. A set of measures of centrality based on betweenness. Sociometry 35–41.
FreightWaves, 2019. Freightwaves website. https://www.freightwaves.com/news/air-cargos-year-end-and-preview-of-2020. Accessed: December 2019.
Girvan, M., Newman, M.E., 2002. Community structure in social and biological networks. Proc. Nat. Acad. Sci. 99 (12), 7821–7826.
Guimera, R., Amaral, L.A.N., 2004. Modeling the world-wide airport network. Eur. Phys. J. B 38 (2), 381–385.
Guimera, R., Mossa, S., Turtschi, A., Amaral-Nunes, L.A., 2005. The worldwide air transportation network: Anomalous centrality, community structure, and cities' global roles. Proc. Nat. Acad. Sci. 102 (22), 7794–7799.
IAR, 2019. International airport review website. https://www.internationalairportreview.com/news/83637/brussels-airports-february-numbers-severely-impacted-by-national-strike/. Accessed: March 2019.
IATA, 2020a. IATA website. https://www.iata.org/contentassets/4d3961c878894c8a8725278607d8ad52/air-cargo-brochure.pdf. Accessed: April 2020.
IATA, 2020b. IATA website. https://www.iata.org/en/programs/cargo/sustainability/benefits/. Accessed: April 2020.
Kaluza, P., Kölzsch, A., Gastner, M.T., Blasius, B., 2010. The complex network of global cargo ship movements. J. Roy. Soc. Interface 7 (48), 1093–1103.
Lakew, P.A., 2014. Economies of traffic density and scale in the integrated air cargo industry: The cost structures of FedEx Express and UPS Airlines. J. Air Transp. Manage. 35, 29–38.
LATAM, 2019. LATAM website. http://www.latamairlinesgroup.net/static-files/ed167ee1-a21d-4fa4-9b17-a231f9a4ebdc. Accessed: September 2019.
Latora, V., Marchiori, M., 2002. Is the Boston subway a small-world network? Physica A 314 (1–4), 109–113.
Lordan, O., Sallan, J.M., Simo, P., Gonzalez-Prieto, D., 2014. Robustness of the air transport network. Transp. Res. Part E: Logist. Transp. Rev. 68, 155–163.
Malighetti, P., Martini, G., Redondi, R., Scotti, D., 2019. Air transport networks of global integrators in the more liberalized Asian air cargo industry. Transp. Policy 80, 12–23.
Malighetti, P., Paleari, S., Redondi, R., 2008. Connectivity of the European airport network: "Self-help hubbing" and business implications. J. Air Transp. Manage. 14 (2), 53–65.
Newman, M.E.J., Girvan, M., 2004. Finding and evaluating community structure in networks. Phys. Rev. E 69 (2), 026113.
Opsahl, T., Panzarasa, P., 2009. Clustering in weighted networks. Soc. Netw. 31 (2), 155–163.
Paleari, S., Redondi, R., Malighetti, P., 2010. A comparative study of airport connectivity in China, Europe and US: which network provides the best service to passengers? Transp. Res. Part E: Logist. Transp. Rev. 46 (2), 198–210.
Petreska, I., Tomovski, I., Gutierrez, E., Kocarev, L., Bono, F., Poljansek, K., 2010. Application of modal analysis in assessing attack vulnerability of complex networks. Commun. Nonlinear Sci. Numer. Simul. 15 (4), 1008–1018.
PlaneStats, 2019. Planestats website. https://www.planestats.com/iataf_2014dec. Accessed: September 2019.
Sen, P., Dasgupta, S., Chatterjee, A., Sreeram, P.A., Mukherjee, G., Manna, S.S., 2003. Small-world properties of the Indian railway network. Phys. Rev. E 67 (3), 036106.
Strogatz, S.H., 2001. Exploring complex networks. Nature 410 (6825), 268.
UPS Pressroom, 2020. UPS Pressroom website. https://pressroom.ups.com/pressroom/ContentDetailsViewer.page?ConceptType=PressReleasesid=1517836912556-134. Accessed: January 2020.
Verma, T., Araújo, N.A.M., Herrmann, H.J., 2014. Revealing the structure of the world airline network. Scient. Rep. 4, 5638.
Wang, J., Mo, H., Wang, F., Jin, F., 2011. Exploring the network structure and nodal centrality of China's air transport network: A complex network approach. J. Transp. Geogr. 19 (4), 712–721.
Watts, D.J., Strogatz, S.H., 1998. Collective dynamics of "small-world networks. Nature 393 (6684), 440.
Yen, J.Y., 1970. An algorithm for finding shortest routes from all source nodes to a given destination in general networks. Q. Appl. Math. 27 (4), 526–530.